Icarus 218 (2012) 585–601

Contents lists available at SciVerse ScienceDirect

Icarus

journal homepage: www.elsevier.com/locate/icarus

The effect of high temperatures on the mid-to-far-infrared emission and near-infrared reflectance spectra of phyllosilicates and natural zeolites: Implications for martian exploration

Congcong Che *, Timothy D. Glotch

Department of Geosciences, 255 ESS Building, Stony Brook University, Stony Brook, NY 11794-2100, United States

ARTICLE INFO

Article history:
Received 28 June 2011
Revised 21 December 2011
Accepted 13 January 2012
Available online 28 January 2012

Keywords:
Mars
Mineralogy
Spectroscopy

ABSTRACT

Most phyllosilicates on Mars appear to be associated with ancient terrains. As such, they may have experienced shock heating produced by impacts and could have been significantly altered or melted. We characterized the effects of high temperatures on the mid-to-far-infrared (mid-to-far-IR) emission (100–1400 cm^{-1}; 7.1–100 μm) and near-infrared (NIR) reflectance (1.2–2.5 μm) spectra of phyllosilicates by measuring experimentally calcined (100–900 °C) phyllosilicates and also two zeolites. Correlated differential scanning calorimetry (DSC) measurements were also performed on each sample to provide insight into the thermal activities of the phyllosilicates and natural zeolites. Our results indicate that all phyllosilicates exhibit characteristic degradations in both NIR and mid-to-far-IR spectral properties between 400 and 800 °C, mainly attributable to the dehydroxylation and recrystallization processes as temperature increases. Spectral features of natural zeolites persist to higher temperatures compared to features of phyllosilicates during heating treatments. The thermal behaviors of phyllosilicate infrared (IR) properties are greatly influenced by the compositions of the octahedral cations: (1) changes in both the NIR and mid-to-far-IR spectra of phyllosilicates tend to occur at lower temperatures (300–400 °C) in the Fe^{3+}-rich samples as compared to the Al^{3+}-rich types (400–600 °C); (2) Mg^{2+}-trioctahedral phyllosilicates hectorite, saponite, and sepiolite all display major mid-to-far-IR spectral changes at 700 °C, corresponding to the formation of enstatite; (3) phyllosilicates that have minor replacement of Mg^{2+} for Al^{3+} in octahedral positions (e.g. cheto-type montmorillonite and palygorskite) show an absorption band at ~920 cm^{-1} that becomes strong at 900 °C. Inconsistency between spectral behaviors in the mid-to-far-IR and NIR regions is also discussed for phyllosilicates. Results from this study have provided suggestive evidence for the scenario that some phyllosilicates could lose all original spectral features in mid-to-far-IR region while maintaining their characteristic hydration bands in NIR region in the same temperature range.

1. Introduction

Phyllosilicates detected on the surface of Mars are primarily associated with heavily cratered Noachian terrains (e.g., Poulet et al., 2005; Bibring et al., 2006; Mangold et al., 2007; Michalski and Noe Dobrea, 2007). It has been suggested that at least some phyllosilicates on Mars were likely formed from long-lived hydrothermal systems initiated by impact processes (e.g., Schwenzer and Kring, 2009), while others have suggested that pre-existing phyllosilicates were excavated by repeated impact events (Fairén et al., 2010). Abramov and Kring (2005) modeled an impact-induced hydrothermal system on Mars and the results indicated that temperatures as high as 1200 °C could last for thousands of years in the region of the impact. Fairén et al. (2010) calculated the temperature increases in a transient crater resulting from an impact, and their model showed that temperatures can reach close to 1000 °C in a certain area around the point of impact. In the laboratory, 400–500 °C is sufficient for phyllosilicates to lose their interlayer H_2O and most phyllosilicates can be completely dehydroxylated at 900 °C (e.g., Che et al., 2011). These previous conclusions lead us to propose that phyllosilicates on Mars may have been affected by impact processes, with an emphasis on post-shock heating, and that dehydrated and/or dehydroxylated phyllosilicates may be present on the martian surface.

The process of phyllosilicate dehydration or dehydroxylation may also help explain the apparent disconnect between visible and near-IR (VNIR) and thermal IR (TIR) observations of phyllosilicates on Mars. Data from the Mars Express Observatoire pour la Minéralogie, l'Eau, les Glaces, et l'Activité (MEx/OMEGA) (0.4–5 μm, 0.3–2 km/pixel) and Compact Reconnassaince Imaging

* Corresponding author.
E-mail address: cche@ic.sunysb.edu (C. Che).

0019-1035/$ - see front matter © 2012 Elsevier Inc. All rights reserved.
doi:10.1016/j.icarus.2012.01.005

Spectrometer for Mars (MRO/CRISM) (0.4–3.9 μm, 18 m/pixel) VNIR imaging spectrometers have provided unambiguous evidence for the widespread presence of phyllosilicates (e.g., Poulet et al., 2005; Bibring et al., 2006; Loizeau et al., 2007; Mangold et al., 2007), while global detection of phyllosilicates in the Mars Global Surveyor (MGS) Thermal Emission Spectrometer (TES) data (6–50 μm, ~3 × 8 km/pixel) has remained unclear because it is difficult to distinguish phyllosilicates and amorphous silica-rich phases (e.g., glass or amorphous weathering products) in the truncated spectral range of TES (e.g., Bandfield, 2002; Ruff, 2003; Michalski et al., 2005, 2006; Ruff and Christensen, 2007). However, it may be possible to identify these minerals at local scales. The phyllosilicate deposits in Nili Fossae detected by OMEGA exhibited different spectral features from surrounding regions in Thermal Emission Imaging System (THEMIS, 6–15 μm, 100 m/pixel) images (McDowell and Hamilton, 2007a,b). The THEMIS phyllosilicate index of Viviano and Moersch (2011) also indicated that THEMIS may be able to provide more reliable phyllosilicate abundance than TES because of its higher spatial resolution. The bright and dark terrains around Mawrth Vallis show distinct spectral character in TES data, in which the dark terrain is consistent with TES Surface Type 1 (ST1, Bandfield et al., 2000) while the bright terrain is clearly different. In the Mawrth Vallis phyllosilicate deposits, TES spectra show evidence for significant abundances of poorly crystalline silica that may be actual opaline silica or a spectroscopic substitution for poorly crystalline phyllosilicates (Michalski and Fergason, 2009). Also in the Nili Fossae region, recent work by Michalski et al. (2010) shows that it is possible to identify phyllosilicate deposits from their long-wavelength spectral features. TES data consistently show a spectral absorption located near 450 cm^{-1} within the same surfaces where OMEGA and CRISM show phyllosilicate occurrences around Nili Fossae. While the presence of these features is consistent with the occurrence of Fe^{2+}-bearing phyllosilicates and/or poorly crystalline Fe/Mg-rich clays, the overall TES spectrum of these surfaces lacks other diagnostic bands normally associated with phyllosilicates: Si–O stretching features in the 900–1100 cm^{-1} region. In summary, TES TIR and OMEGA/CRISM VNIR spectra give different perspectives on phyllosilicate mineralogy, crystallinity, and abundance on Mars. Among the potential reasons for this disconnect is the possibility that phyllosilicates on Mars have been modified by the effects of dehydration and/or dehydroxylation. Such effects modify the mineral structures in such a way that their spectroscopic signatures appear different from various wavelength-perspectives. Laboratory spectral studies of dehydrated or dehydroxylated phyllosilicates are essential to characterize how high temperatures affect NIR and TIR spectra in different ways.

The effects of high temperatures on VNIR reflectance spectra of several types of phyllosilicates (including montmorillonites and nontronites) were studied previously (e.g., Milliken and Mustard, 2005; Fairén et al., 2010; Gavin and Chevrier, 2010). In general, these laboratory studies showed that VNIR spectra of phyllosilicates change distinctly as temperature increases and become mostly featureless because of the dehydroxylation process at temperatures above 700 °C. However, there is no substantive work that thoroughly describes the mid-to-far-IR emissivity spectra of dehydrated and/or dehydroxylated phyllosilicates. A detailed study was carried out on the attenuated total reflectance (ATR) and mid-to-far-IR specular reflectance of dehydrated and/or dehydroxylated phyllosilicates by Che et al. (2011). The reflectance spectra can be used to approximate emissivity spectra using Kirchhoff's Law ($E = 1 - R$). However, Kirchhoff's Law only holds true when the surface is a Lambertian scatterer (e.g., Salisbury et al., 1994), so laboratory mid-to-far-IR reflectance spectra may have limitations when applied to analysis of data from the non-Lambertian martian surface. In this study we present the mid-to-far-IR emissivity and NIR reflectance spectra of dehydrated and/or dehydroxylated phyllosilicates (from the same suite of samples as in Che et al., 2011). These samples come from four structural groups: kaolinite, smectite, chlorite, and palygorskite–sepiolite. In addition to phyllosilicates, two natural zeolite samples were included in this study. Zeolites are also important hydrous minerals identified on Mars (e.g., Ruff, 2004; Ehlmann et al., 2009) and they have similar chemical compositions to phyllosilicates. Analysis of zeolite samples can help provide a more comprehensive database for characterizing how the mid-to-far-IR emissivity and NIR reflectance spectra of alumino-silicates change upon heating. The aim in this research is to (1) establish both mid-to-far-IR emissivity and NIR reflectance spectral libraries for identification of possible dehydrated/or dehydroxylated phyllosilicates on Mars, and (2) compare the spectral changes in the mid-to-far-IR region with those in the NIR region to characterize the different trends that could lead to the apparent disconnect between mid-to-far-IR and NIR detection of phyllosilicates on Mars.

2. Methods

2.1. Sample description, preparation, and characterization

In this study we collected the mid-to-far-IR emissivity spectra and NIR reflectance spectra of the same suite of phyllosilicates and natural zeolites from Che et al. (2011) (Table 1). All samples were purchased from the Clay Mineral Society (CMS) Source Clay Repository unless otherwise stated. Chemical compositions for these samples are summarized in Table 2. To facilitate precise characterization of all samples, the phyllosilicates and natural zeolites were prepared to <2 μm size fractions prior to heat treatments. The phyllosilicates and natural zeolites were then heated for 24 h to 100, 200, 300, 400, 500, 600, 700, 800, and 900 °C. To minimize the effects of rehydration processes, all heated products were stored in a desiccator before the spectral measurements and a purge gas system was used to remove CO_2 and water vapor from the spectrometer. Details of the preparation and X-ray diffraction (XRD) characterization of phyllosilicates and natural zeolites used for this work were reported in Che et al. (2011).

2.2. Differential scanning calorimetry measurements (DSC)

DSC measures the difference in heat required to maintain isothermal conditions between the sample and an inert reference at the same temperature (e.g., Hedley et al., 2007). DSC can be used to study the thermal reactions (e.g. endothermic and exothermic reactions) of phyllosilicates and natural zeolites during dehydration and/or dehydroxylation processes. In this study, DSC analyses of all phyllosilicates and natural zeolites were carried out in order to record thermal activity of each sample. We collected DSC curves of all size-separated samples by heating them from 25 °C to 1000 °C at 10 °C min^{-1} using a Netzsch Simultaneous TG-DTA/DSC Apparatus Model STA 449C analyser. All DSC curves were recorded in a N_2-protected environment. We relate the thermal behaviors of the phyllosilicates and zeolites with their IR spectral properties using DSC curves in Section 4.

2.3. Infrared spectroscopic measurements

The NIR diffuse reflectance and mid-to-far-IR emissivity spectra were acquired at Stony Brook University in the Vibrational Spectroscopy Laboratory (VSL) using a Nicolet 6700 FTIR spectrometer produced by Thermo Fisher. Each sample was pressed in a Carver hydraulic press at ~18,000 PSI to create a pellet, 13 mm in

Table 1
Summary of phyllosilicates and zeolites for this study.[a]

Structural group	Mineral	Sample number	Source	Size fraction
Smectite group	"Cheto" montmorillonite	SAz-1	CMS	<2 μm
	Texas montmorillonite	STx-1	CMS	<2 μm
	Na-montmorillonite (Wyoming)	SWy-2	CMS	<2 μm
	Montmorillonite (Otay)	SCa-3	CMS	<2 μm
	Mica-montmorillonite	Syn-1	CMS	<2 μm
	Beidellite	SBCa-1	CMS	<2 μm
	Hectorite	SHCa-1	CMS	<2 μm
	Saponite	SapCa-2	CMS	<2 μm
	Nontronite	NAu-1	CMS	<2 μm
	Nontronite	NAu-2	CMS	<2 μm
Kaolinite–serpentine group	Kaolinite	KGa-1b	CMS	<2 μm
Sepiolite–palygorskite group	Sepiolite	SepSp-1	CMS	<2 μm
	Palygorskite (Attapulgite)	PFl-1	CMS	<2 μm
Chlorite group	Clinochlore	Clinochlore	Mineral Unlimited	<2 μm
Zeolite group	Mordenite	27,133	Mineral Research	<2 μm
	Clinoptilolite	27,031	Mineral Research	<2 μm

[a] Table adopted from Che et al. (2011).

Table 2
Summary of major elemental composition.[a]

Sample number	SiO_2	Al_2O_3	Fe_2O_3	FeO	TiO_2	MgO	CaO	Na_2O	K_2O	P_2O_5	OH/H_2O[b]
SAz-1[c]	51.36	17.20	1.54	n.a.	0.22	5.80	2.71	0.05	0.16	0.01	20.96
STx-1[c]	63.36	16.17	1.09	n.a.	0.24	3.43	1.57	0.28	0.06	0.01	13.78
SWy-2[c]	56.08	20.12	3.99	n.a.	0.08	2.68	1.08	1.34	0.18	0	14.45
SCa-3[d]	55.78	12.47	1.53	n.a.	n.a.	8.55	0.04	2.84	n.a.	n.a.	18.78
Syn-1[c]	47.70	36.75	0.11	n.a.	0.03	0.17	0.05	0.08	0	0	14.91
SBCa-1[e]	51.03	30.71	2.34	0.11	0.57	1.03	1.11	<0.01	0.79	0.12	12.17
SHCa-1[c]	46.11	0.85	0.32	n.a.	0.04	19.77	13.84	1.33	0.14	0	17.60
NAu-1[5]	41.55	6.59	29.07	n.a.	0.02	0.15	2.89	0.02	0.01	n.a.	19.70
NAu-2[f]	49.52	2.74	33.36	n.a.	0.02	0.23	2.06	0.12	0.01	n.a.	11.94
SapCa-2[g]	53.33	4.60	1.19	n.a.	0.09	24.49	1.30	1.19	0.19	n.a.	13.63
KGa-1b[h]	43.98	38.22	0.20	n.a.	1.62	0.06	0.03	0.03	0.02	n.a.	15.84
SepSp-1[i]	55.00	1.40	0.40	0.02	0.04	22.38	1.07	<0.15	0.20	<0.05	19.29
PFl-1[c]	54.33	10.02	3.37	n.a.	0.43	9.52	1.70	0.05	0.78	0.83	18.97
Clinochlore[j]	26.38	29.24	1.64	5.05	n.a.	25.36	n.a.	n.a.	n.a.	n.a.	12.34
27133[k]	67.06	15.51	n.a.	n.a.	n.a.	0.37	3.10	3.92	0.51	n.a.	12.58
27031[l]	61.94	11.97	2.12	n.a.	0.23	1.61	0.91	4.02	1.54	n.a.	15.55

n.a. = not analyzed.
[a] Table adopted from Che et al., 2011.
[b] OH/H_2O takes as total weight loss on ignition (after heating sample to 1000 °C).
[c] Mermut and Faz Cano (2001).
[d] Van olphen and Fripiat (1979).
[e] Unofficially reported by CMS: http://www.clays.org/SOURCE%20CLAYS/SCdata.html.
[f] Keeling et al. (2000).
[g] Post (1984).
[h] Pruett and Webb (1993).
[i] USGS Digital Spectral Library: http://speclab.cr.usgs.gov/spectral.lib04/DESCRIPT/sepiolite.SepSp-1.html.
[j] Ballet et al. (1985).
[k] http://www.handbookofmineralogy.org/pdfs/mordenite.pdf.
[l] Bish (1984).

diameter and about 3 mm in thickness. This method has been used previously to prepare phyllosilicate samples for analysis by emission and specular reflectance spectroscopy (e.g., Michalski et al., 2005; Glotch et al., 2007). The purpose of pressing the samples into pellets with smooth surfaces is to minimize the spectral effects caused by physical properties, such as surface roughness and particle size (Michalski et al., 2005). Therefore the spectral measurements of pressed samples could allow us to focus on the spectral differences among the phyllosilicates induced by their mineralogical properties. Although spectral laboratory studies of pelletized phyllosilicates may not be applied to the analysis of finely particulate phyllosilicates on Mars, previous work showed that the spectral features of pellet samples could be used for remote sensing of phyllosilicates occurring as coarse particles or indurated materials (Michalski et al., 2005).

2.3.1. NIR diffuse reflectance spectra

The NIR reflectance spectra (1.2–2.5 μm) were collected for all samples and their heated products using a Thermo Fisher diffuse reflectance accessory. Spectra were ratioed to a gold mirror standard. For these measurements, the spectrometer was equipped with a CaF_2 beamsplitter and an InGaAs detector. For each sample, 2048 scans in the NIR spectral range were recorded with a resolution of 4 cm^{-1}.

2.3.2. Emissivity spectra

Emissivity spectra in the mid-to-far-IR (100–2000 cm^{-1}, 100–5 μm) range were acquired by switching off the Globar IR source and measuring the radiation from the heated samples directly. The samples were heated and maintained at 80 °C to provide adequate signal for the measurements. A blackbody heated to 70 °C

and 100 °C was used to calibrate the emissivity spectra in the manner of Ruff et al. (1997). Spectra from 400 to 2000 cm^{-1} were acquired at 4 cm^{-1} resolution using a KBr beamsplitter and a DLaTGS detector with a KBr window. A total of 512 scans were averaged to produce each spectrum. Far-IR spectra were collected from 100 to 600 cm^{-1} using a Thermo Fisher Solid Substrate beamsplitter and a DLaTGS detector. A total of 2048 scans and 4 cm^{-1} resolution were used for this spectral range. The emissivity spectra were obtained for all samples and their heated products.

3. Results

3.1. Differential thermal investigation: DSC

DSC results for phyllosilicates and natural zeolites studied here are illustrated in Fig. 1. The endothermic or exothermic peaks shown in DSC curves are important features associated with physical or chemical transformation with a thermal effect. In Fig. 1 the endothermic and exothermic activities of each sample are identified as absorption features and peak features, respectively.

In general, kaolinite (Fig. 1a) and clinochlore (Fig. 1n) both show two strong endothermic effects at ~600 °C and ~800 °C. The other 14 samples all exhibit an endothermic feature near 100 °C and distinct thermal activity features in the higher temperature range (200–1000 °C). The DSC curves of minerals from the same structural group resemble each other in shape but not in details. For example, DSC curves of PFl-1 palygorskite (Fig. 1l) and SepSp-1 sepiolite (Fig. 1m) are both characterized by a multistep endothermic process at temperatures lower than 600 °C and an endothermic–exothermic inversion feature near 850 °C. The temperature and extent of each reaction, however, are different for these two samples. This is also found to be the case for nontronites NAu-1 and NAu-2 (Fig. 1f and g), samples SBCa-1 and Syn-1 (Fig. 1j and k) with a beidellite composition (Kloprogge et al., 1999a), and natural zeolites 27,031 and 27,133 (Fig. 1o and p). In the case of montmorillonites, STx-1 sample (Fig. 1d) gives a DCS curve similar to the SWy-2 sample (Fig. 1e) while DSC patterns for SAz-1 and SCa-3 montmorillonites differ from the previous two montmorillonite samples.

3.2. Mid-to-far-IR emissivity spectra

Spectral features in the mid-to-far-IR region are dominated by fundamental molecular vibration bands and are a particularly important indicator of mineralogy and chemical composition for the major rock-forming minerals (e.g., Salisbury, 1993). Spectral features of phyllosilicates in this region and their interpretations have been studied comprehensively by numerous authors (e.g., Farmer, 1974; Van der Marel and Beutelspacher, 1976; Kloprogge et al., 1998, 1999a,b, 2000; Frost and Kloprogge, 2000; Frost

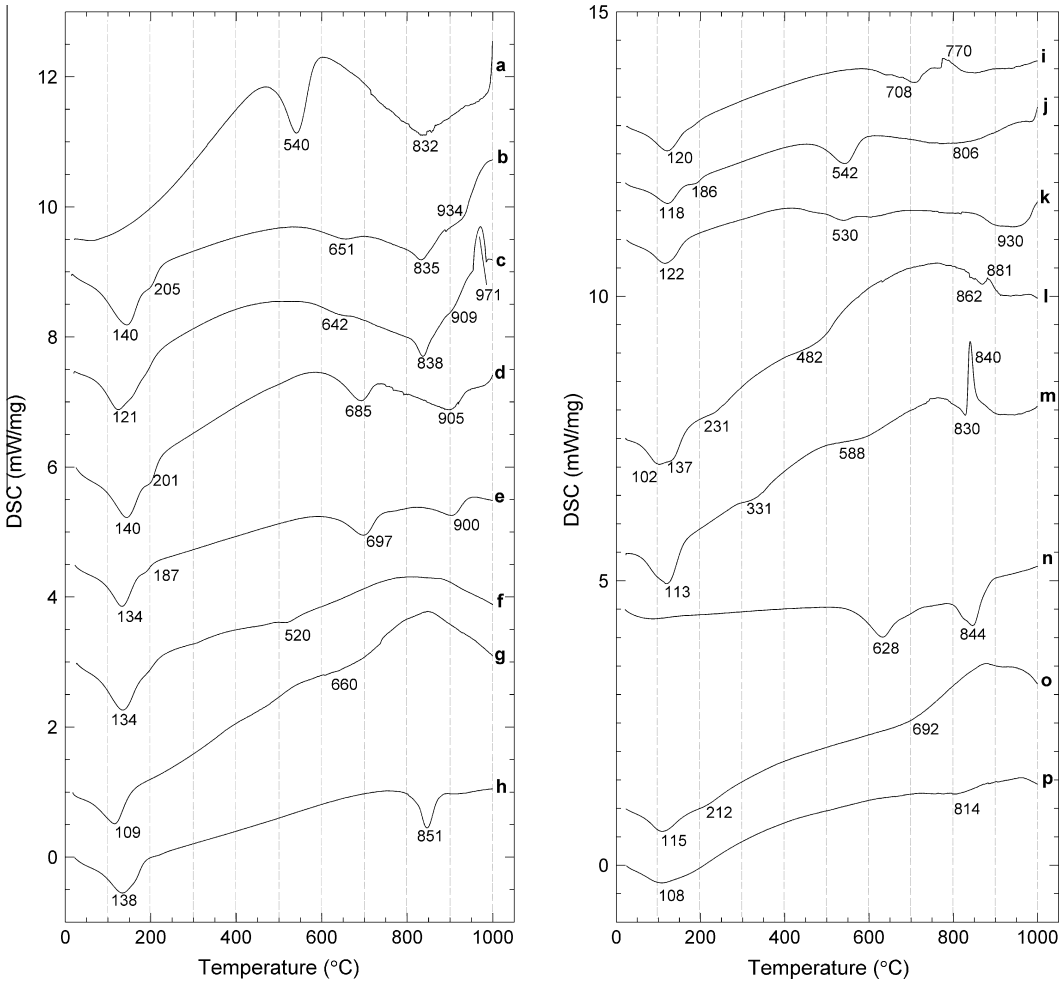

Fig. 1. DSC curves (offset) of (a) KGa-1b kaolinite, (b) SAz-1 "Cheto" montmorillonite, (c) SCa-3 montmorillonite (Otay), (d) STx-1 Texas montmorillonite, (e) SWy-2 Na-montmorillonite (Wyoming), (f) NAu-1 nontronite, (g) NAu-2 nontronite, (h) SapCa-2 saponite, (i) SHCa-1 hectorite, (j) SBCa-1 beidellite, (k) Syn-1 mica-montmorillonite, (l) PFl-1 palygorskite, (m) SepSp-1 sepiolite, (n) clinochlore, (o) 27,031 clinoptilolite, and (p) 27,133 mordenite.

et al., 2002; Madejová and Komadel, 2001; Michalski et al., 2005; Bishop et al., 2008; Che et al., 2011). In general, absorption bands near 1200–1000 cm^{-1} are due to Si–O stretching motions in the tetrahedral sheets, spectral features near 550–400 cm^{-1} are associated with Si–O bending vibrations in the tetrahedral sheets and M–O–Si (M = Al^{3+}, Fe^{3+}, Fe^{2+}, or Mg^{2+} in the octahedral sheets) deformation modes, and spectral bands observed in the 950–590 cm^{-1} range are related to M–OH or M–M–OH bending vibrations in octahedral sheets. Spectral features in the far-IR region (<400 cm^{-1}) are assigned to the interlayer cations and mixed vibrations that include the Si–O network, octahedral cations, and hydroxyl groups. It is noteworthy that the ~1600 cm^{-1} spectral feature due to H–O–H bending vibration is extremely weak, due to the use of pelletized samples (e.g., Salisbury, 1993). As a result, the 1400–2000 cm^{-1} region of the spectrum appears featureless. Therefore the subsequent figures only show the 100–1400 cm^{-1} region of the spectrum.

3.2.1. Kaolinite group

For kaolinite (Fig. 2), the multiple spectral bands occurring near 1200–1000 cm^{-1} and 550–400 cm^{-1} change significantly upon heating. At 400 °C they are replaced by new bands near 1067 cm^{-1} and 440 cm^{-1}, respectively. These two new absorption features shift gradually to higher wavenumbers with increasingly higher temperatures. These two bands also become narrower at 800 °C. As with the spectral features in the mid-IR region (1400–400 cm^{-1}), spectral bands in the far-IR region disappear at 400 °C. No new bands are observed at higher temperatures in this region.

3.2.2. Smectite group

Fig. 3 shows mid-to-far-IR emissivity spectra for four montmorillonite samples (a fifth sample, Syn-1 mica-montmorillonite is discussed later with the beidellite sample SBCa-1, because a previous study (Kloprogge et al., 1999a) indicates that both its chemical composition and spectral features are close to those for beidellite.) and their Si–O stretching bands are all composed of a strong absorption feature near 1065 cm^{-1} and a weak shoulder absorption feature near 1130 cm^{-1}. The shoulder absorption feature becomes stronger as temperature is increased and at 600 °C, it develops into an absorption feature with a detectable intensity. However, this feature becomes weak again at 700 °C for SAz-1 and SCa-3 montmorillonites, then disappears completely at 800 °C for all four montmorillonites. The strong Si–O stretching band of the four montmorillonites disappears and is replaced by a new strong band at ~1100 cm^{-1} at 800 °C. At 900 °C, this 1100 cm^{-1} feature displays a distinct shift towards high wavenumbers for the SAz-1 and SCa-3 samples while showing no change for STx-1 and SWy-2. In the Si–O bending region, all montmorillonite samples exhibit a doublet feature at ~470 and ~530 cm^{-1}, which is completely lost and replaced by a strong band (~490 cm^{-1}) with two weak shoulders (~570 and ~420 cm^{-1}) at 500 °C (600 °C for SWy-2). At 800 °C, these shoulder spectral bands disappear and the new strong feature shifts to lower wavenumbers. Therefore, the Si–O bending region of all four montmorillonites has a strong absorption near 460 cm^{-1} at 800 °C. No additional changes occur to this strong feature for STx-1 and SWy-2 at 900 °C. However, this 460 cm^{-1} spectral feature becomes significantly stronger and shifts to lower wavenumbers (~425 cm^{-1}) for SAz-1 and SCa-3. A weak spectral band at ~330 cm^{-1} is observed for all montmorillonites. This feature shifts to lower wavenumbers (~300 cm^{-1}) at 500 °C (600 °C for SWy-2 montmorillonite) and disappears completely at 800 °C.

For the two nontronite samples (Fig. 4a: NAu-1 and Fig. 4b: NAu-2) in this study, the multiple Si–O stretching features near 1100 cm^{-1} are replaced by a strong absorption band at ~1080 cm^{-1} upon heating to 400 °C. This new feature continually shifts towards higher wavenumbers with increasing temperature. It is also important to note that a new shoulder feature develops near 1200 cm^{-1} at 800 °C for both nontronite samples. The Si–O bending bands of the nontronite samples disappear and forming a single new feature near 450 cm^{-1}. At 800 °C this new band becomes narrower and shows a slight shift to higher wavenumbers (~470 cm^{-1}). Two nontronite samples both display multiple weak features in the 400–200 cm^{-1} range. At 400 °C these bands are lost and replaced by a weak band near 310 cm^{-1}. This weak feature then disappears at 800 °C.

Only one main spectral change is observed for SapCa-2 saponite (Fig. 5) during the heating treatment. Upon heating to 700 °C, the spectrum of saponite exhibits completely different features from those at 600 °C. These new bands become stronger as temperature is increased. SHCa-1 hectorite (Fig. 6) has a similar spectral behavior to saponite, which includes the disappearance of the original spectral bands and appearance of multiple spectral features in Si–O stretching, Si–O bending and far-IR regions at 700 °C. These new features become stronger upon heating to 900 °C.

For SBCa-1 beidellite (Fig. 7a), two spectral bands in the Si–O stretching region continuously shift away from each other with an increase in temperature. At 900 °C these two bands are replaced by single strong absorption near 1100 cm^{-1}. In the Si–O bending region, SBCa-1 shows only a minor change upon heating to 800 °C; the 546 cm^{-1} band becomes weak at 400 °C and then gradually shifts to high wavenumbers. At 900 °C, the original spectral band disappears and the spectrum exhibits a strong feature at ~463 cm^{-1} with a weak feature at ~555 cm^{-1} in the Si–O bending region. The 338 and 255 cm^{-1} bands of beidellite are lost at 400 °C. A new feature at ~307 cm^{-1} then forms at 500 °C and eventually disappears at 900 °C. In the case of Syn-1 montmorillonite (Fig. 7b), the spectral features all show slight changes in intensities

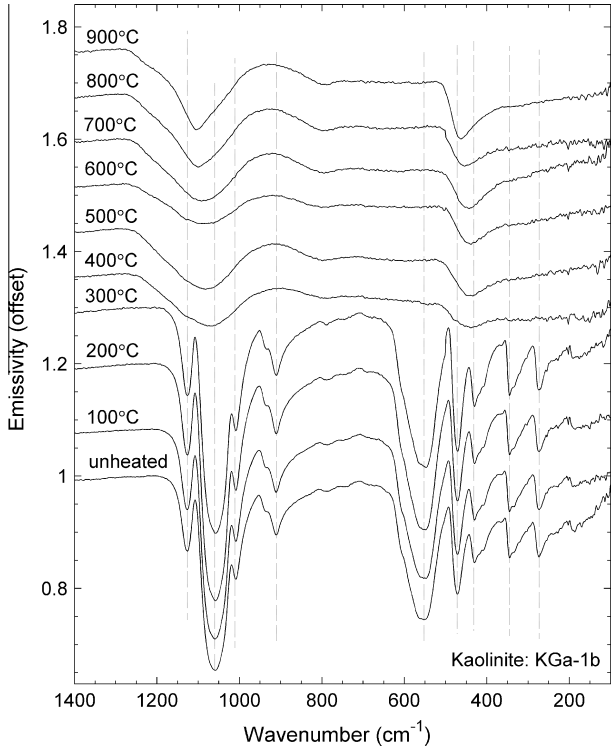

Fig. 2. 100–1400 cm^{-1} emissivity spectra of kaolinite (KGa-1b) calcined at various temperatures. Linear vertical offset is applied to the spectra for clarity.

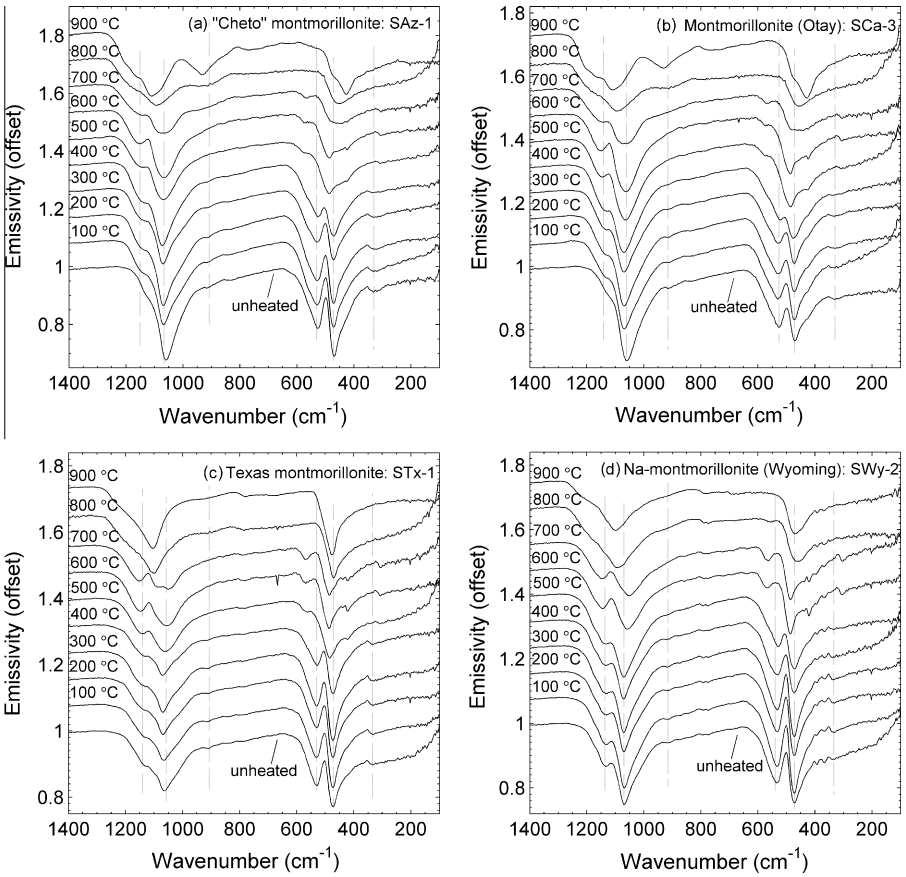

Fig. 3. (a) 100–1400 cm^{-1} emissivity spectra of "Cheto" montmorillonite (SAz-1) calcined at various temperatures. (b) 100–1400 cm^{-1} emissivity spectra of montmorillonite (Otay) (SCa-3) calcined at various temperatures. (c) 100–1400 cm^{-1} emissivity spectra of Texas montmorillonite (STx-1) calcined at various temperatures. (d) 100–1400 cm^{-1} emissivity spectra of Na-montmorillonite (Wyoming) (SWy-2) calcined at various temperatures. Linear vertical offset is applied to the spectra for clarity.

and positions upon heating. Besides these, the spectral bands of Syn-1 remain stable to 900 °C.

3.2.3. Sepiolite–palygorskite group

Two distinct spectral changes are observed for palygorskite (Fig. 8a) in the Si–O stretching region upon heating. At 300 °C the spectral features near 1200–1000 cm^{-1} combine together to form a new band centered at ~1050 cm^{-1}. At 800 °C this new feature shifts significantly toward high wavenumbers and ending up near 1103 cm^{-1} at 900 °C. The three spectral bands of sepiolite (Fig. 8b) in the Si–O stretching region behave differently with heating, then at 700 °C they are replaced by a single absorption feature at ~1035 cm^{-1}. Upon heating to 800 °C, the single absorption feature shows a dramatic change, being replaced by several bands over the range 900–1200 cm^{-1}. The Si–O bending bands of palygorskite are lost at 400 °C and are replaced by a broad 450 cm^{-1} feature plus a weak shoulder feature at ~550 cm^{-1}. Upon heating to 800 °C, palygorskite loses the spectral features developed at 400 °C and exhibits a strong new feature at ~465 cm^{-1}. The intensities and band positions of sepiolite spectral features in the Si–O bending region show several steps of changes upon heating (at 300, 700, 800 °C, respectively), the most distinct spectral change occurring at 800 °C. At temperatures lower than 800 °C, the complex spectral bands of sepiolite in the Si–O bending region are centered at ~480 cm^{-1}. At 800 °C new spectral bands are developed at higher wavenumbers (centered at ~520 cm^{-1}). The spectral change in far-IR region for palygorskite is difficult to observe due to water vapor present in the spectrum, but no major bands appear to be present in this region. In the case of sepiolite, the band at ~365 cm^{-1} disappears and several bands are observed to develop from 400 to 200 cm^{-1} at 800 °C.

3.2.4. Chlorite group

Spectra of clinochlore (Fig. 9) and its heating products show two steps of spectral changes occurring at 500 °C and 800 °C. At 500 °C, the original Si–O stretching bands combine together to form a single feature at ~1080 cm^{-1}, which disappears completely at 800 °C. In the Si–O bending region, at 500 °C all original features disappear and are replaced by a strong band at 476 cm^{-1}. At 800 °C this new band splits into multiple spectral features that develop and become stronger at 900 °C. In the far-IR region, a spectral feature at ~370 cm^{-1} becomes very weak at 500 °C and disappears at 800 °C. New multiple spectral features in the 400–200 cm^{-1} region start to develop upon heating to 800 °C.

3.2.5. Zeolite group

The IR spectral properties of zeolites were summarized by previous studies (e.g., Breck, 1974a). The tetrahedral stretching band (~1082 cm^{-1}) of 27,031 clinoptilolite (Fig. 10a) shows no major changes upon heating, although it shifts slightly to higher wavenumbers (1094 cm^{-1}) at 800 °C. In the case of 27,133 mordenite (Fig. 10b), its tetrahedral stretching bands near 1086 cm^{-1} shifts to 1097 cm^{-1} at 800 °C while the shoulder Si (Al)–O stretching band (~1230 cm^{-1}) remains unchanged to 900 °C. The Si (Al)–O bending bands of clinoptilolite (471 cm^{-1}) and mordenite (469 cm^{-1}) are both stable and do not show any distinct spectral change upon heating. In the far-IR region, these two samples

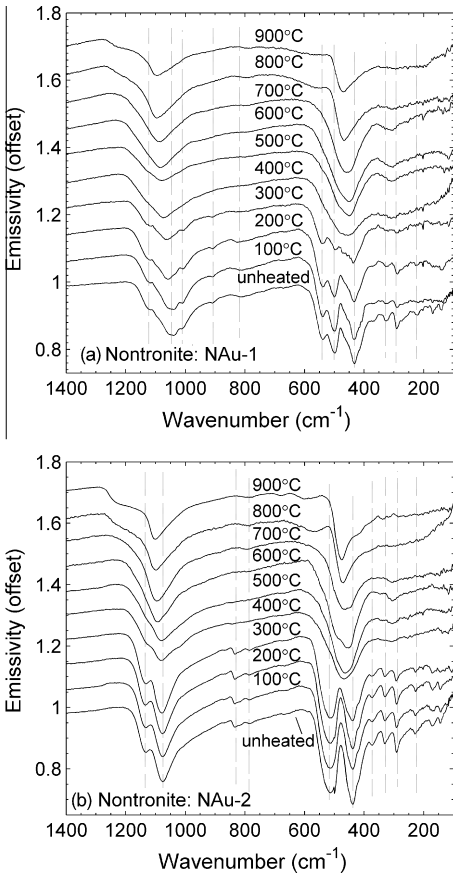

Fig. 4. (a) 100–1400 cm^{-1} emissivity spectra of nontronite (NAu-1) calcined at various temperatures. (b) 100–1400 cm^{-1} emissivity spectra of nontronite (NAu-2) calcined at various temperatures. Linear vertical offset is applied to the spectra for clarity.

display no major spectral features and no new spectral features are observed to form upon heating.

3.2.6. Other observations

The 950–590 cm^{-1} region of phyllosilicates exhibit absorption bands attributable to bending vibration of hydroxyls groups bound to octahedral cations. Overall, the spectra of all sample studied here show that absorption features in this region disappear or become too weak to be identified after the samples are heated to a certain high temperature. For some of the phyllosilicates, however, distinct spectral features appear in this region when samples are heated to 700 °C. Saponite (Fig. 5), hecorite (Fig. 6), and sepiolite (Fig. 8b) exhibit multiple spectral bands near 900 cm^{-1} upon heating to 700 °C (800 °C for sepiolite). For montmorillonites SAz-1 (Fig. 3a), SCa-3 (Fig. 3b), palygorskite (Fig. 8a), and clinochlore (Fig. 9), a single spectral band begins to develop near 900 cm^{-1} at 800 °C, becoming a strong absorption band at 900 °C.

3.3. NIR diffuse reflectance spectra

The NIR (1.2–2.5 μm in this study) is very useful for remote sensing analysis of hydrous minerals, because it is in this region that the minerals have spectral bands due to overtones and combinations of OH and H_2O vibrations. In general, the overtone of the OH stretching modes occurs in the 1.4 μm region, combination modes of H_2O molecules produce the absorptions in the 1.9 μm region, and spectral features near 2.2–2.4 μm regions are due to a combination of the OH stretching and M–OH bending modes (e.g., Gaffey et al., 1993; Bishop et al., 1994).

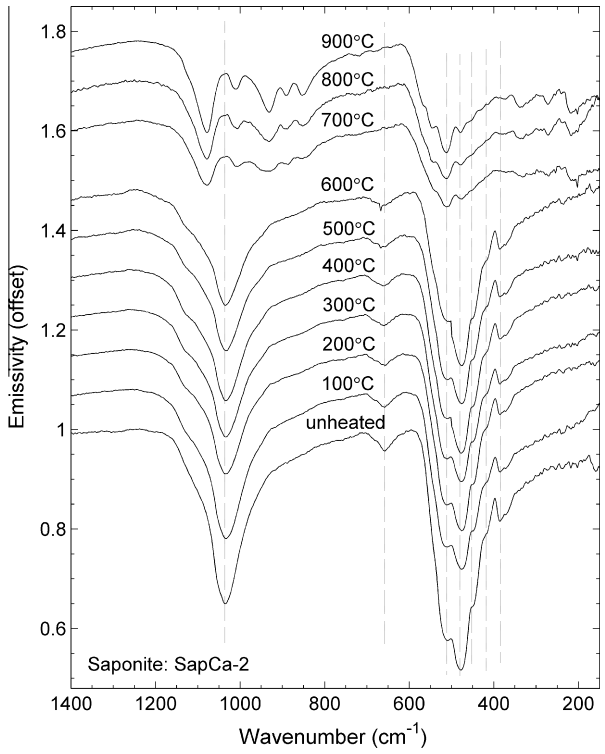

Fig. 5. 150–1400 cm^{-1} emissivity spectra of saponite (SapCa-2) calcined at various temperatures. Linear vertical offset is applied to the spectra for clarity.

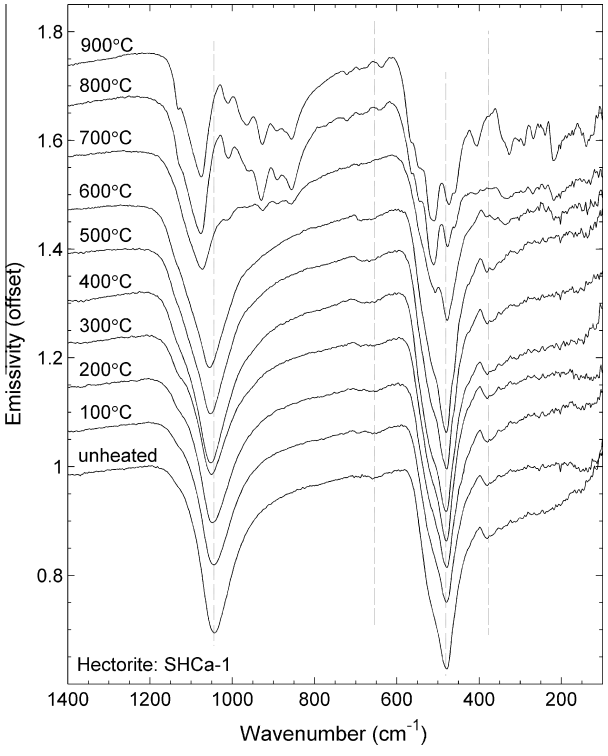

Fig. 6. 100–1400 cm^{-1} emissivity spectra of hectorite (SHCa-1) calcined at various temperatures. Linear vertical offset is applied to the spectra for clarity.

3.3.1. Kaolinite group

Kaolinite (Fig. 11) exhibits strong OH overtones in the 1.4 μm region. These spectral features become weak at 400 °C and then disappear at 700 °C. Upon heating, a very weak spectral band at

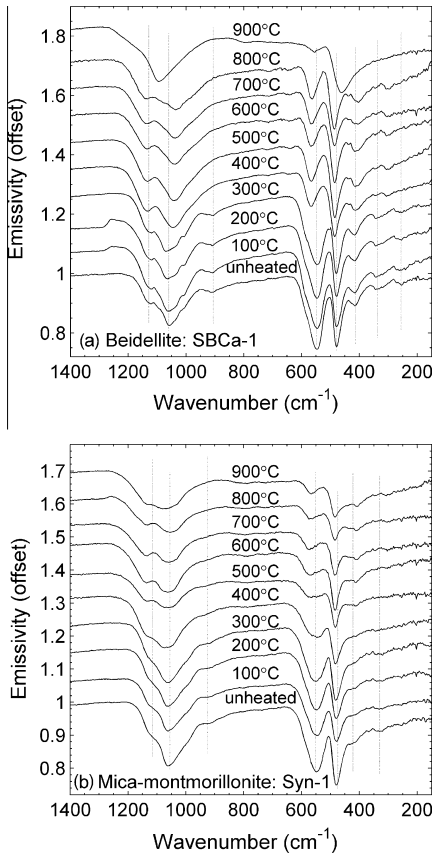

Fig. 7. (a) 150–1400 cm^{-1} emissivity spectra of beidellite (SBCa-1) calcined at various temperatures. (b) 150–1400 cm^{-1} emissivity spectra of mica-montmorillonite (Syn-1) calcined at various temperatures. Linear vertical offset is applied to the spectra for clarity.

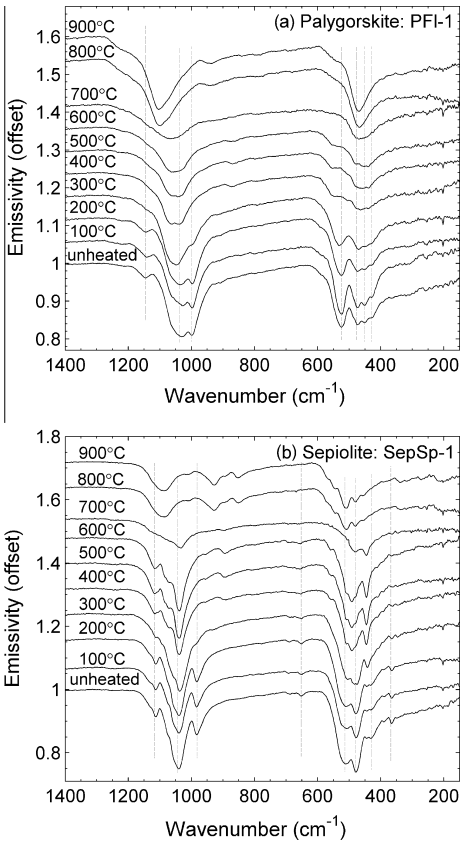

Fig. 8. (a) 150–1400 cm^{-1} emissivity spectra of palygorskite (PFI-1) calcined at various temperatures. (b) 150–1400 cm^{-1} emissivity spectra of sepiolite (SepSp-1) calcined at various temperatures. Linear vertical offset is applied to the spectra for clarity.

1.367 μm appears at 400 °C and it is present in the spectrum until 900 °C. Kaolinite does not have structural H_2O. However, weak spectral features are observed near 1.9 μm, which is probably due to adsorbed water or H_2O associated with impurities in the sample (Bishop et al., 2008). These features are replaced by one weak band at ~1.9 μm upon heating to 400 °C. This weak new feature is present until kaolinite is heated to 900 °C. Kaolinite exhibits 2.16 and 2.21 μm bands due to the AlAlOH combination modes. These two features are replaced by a broad absorption centered at 2.19 μm upon heating to 400 °C. This 2.19 μm band is present in the spectrum until 900 °C.

3.3.2. Smectite group

The 1.410 μm feature of montmorillonites SAz-1 (Fig. 12a) and SCa-3 (Fig. 12b) does not show obvious changes upon heating to 400 °C. At 500 °C, the original band is replaced by two weak absorptions at ~1.365 and ~1.399 μm which both disappear completely at 800 °C. STx-1 (Fig. 12c) displays similar spectral behaviors to SAz-1 and SCa-3. However, the 1.410 μm feature shifts to 1.400 μm at 600 °C and the new 1.366 μm feature of STx-1 is present in the spectrum from 400 to 800 °C. Swy-2 (Fig. 12d) keeps its 1.410 μm feature stable upon heating to 500 °C. In the 600 and 700 °C spectra of SWy-2, two extremely weak absorptions occur at ~1.366 and ~1.396 μm. At 800 °C no major spectral feature is observed in the 1.4 μm region for SWy-2. The 1.9 μm band of SAz-1, SCa-3, STx-1, and Swy-2 montmorillonites each displays slight shifts to shorter wavelengths at 400 °C and decreases in intensity at 700 °C, before disappearing completely upon heating to 800 °C. For the four montmorillonites analyzed here, there are

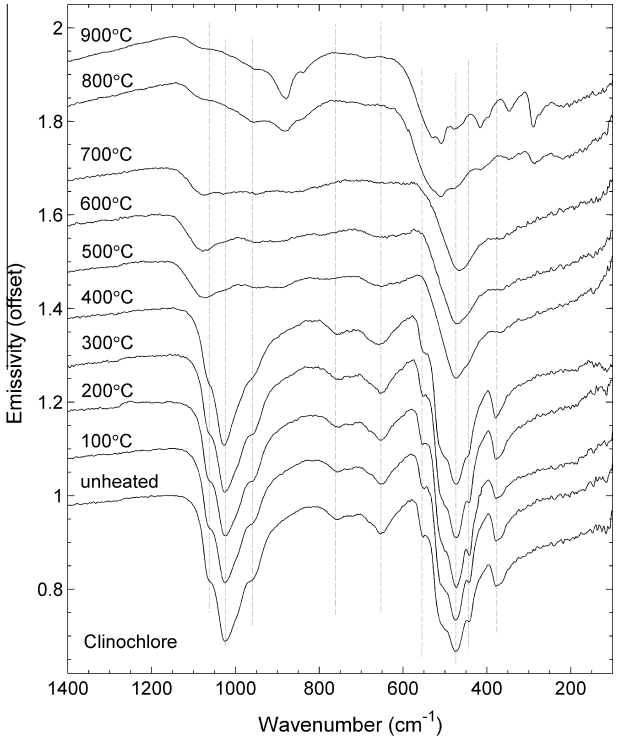

Fig. 9. 100–1400 cm^{-1} emissivity spectra of clinochlore calcined at various temperatures. Linear vertical offset is applied to the spectra for clarity.

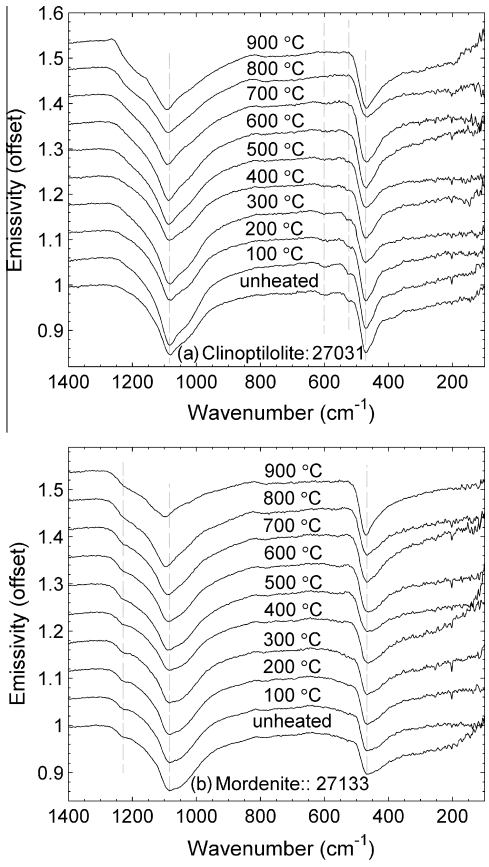

Fig. 10. (a) 100–1400 cm^{-1} emissivity spectra of clinoptilolite (27,031) calcined at various temperatures. (b) 150–1400 cm^{-1} emissivity spectra of mordenite (27,133) calcined at various temperatures. Linear vertical offset is applied to the spectra for clarity.

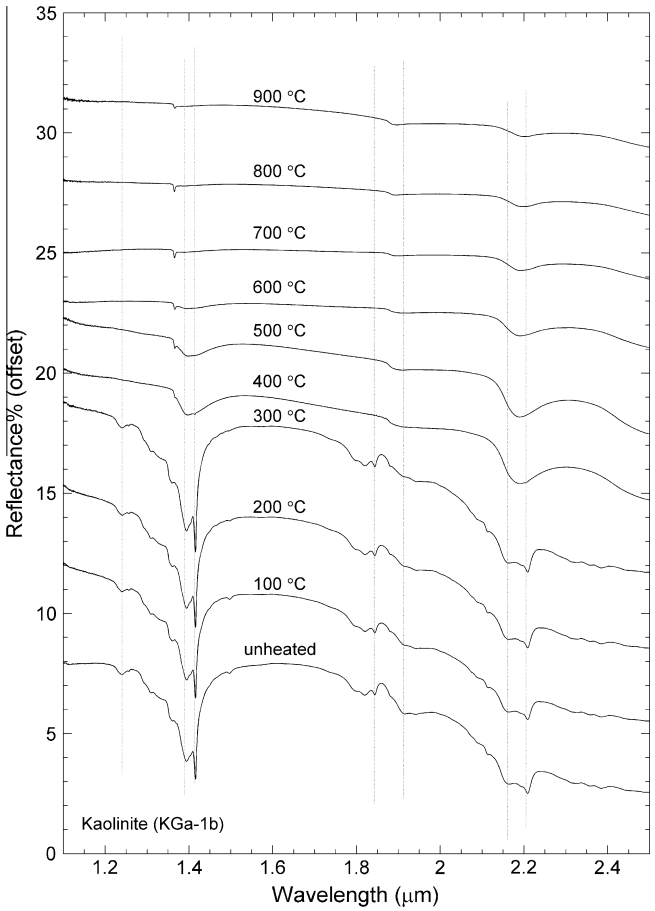

Fig. 11. 1.1–2.5 μm diffuse reflectance spectra of kaolinite (KGa-1b) calcined at various temperatures. Linear vertical offset is applied to the spectra for clarity.

two obvious spectral changes observed in the 2.2 μm region upon heating: the 2.21 μm feature disappears and new bands at ~2.19, ~2.3, and ~2.4 μm begin to develop at 500 °C (600 °C for SWy-2). At 800 °C their spectra only exhibit extremely weak 2.2 μm band and at 900 °C montmorillonites lose all spectral features in the 2.2–2.4 μm region.

For both nontronite samples (Fig. 13a: NAu-1; Fig. 13b: NAu-2) in this study, the bands in 1.4 μm region disappear completely upon heating to 400 °C and no new spectral features appear in the following heating treatments. A strong feature near 1.91 μm is observed for both nontronites in this study. At 400 °C this band is split into two weak absorptions at ~1.91 and ~1.95 μm which then disappear upon heating to 700 °C. The 2.2, 2.3, and 2.4 μm features of the nontronites become very weak and shift slightly away from their original spectral positions at 400 °C, then disappear completely at 700 °C.

The 1.41 μm feature of SapCa-2 saponite (Fig. 14) becomes weak at 100 °C and completely disappears at 200 °C. Saponite also displays a sharp absorption at 1.392 μm, which is observed to be present in the spectrum until 800 °C. During the heating treatment, very weak bands in the 1.38–1.36 μm range accompany the 1.392 μm features. All bands then disappear at 900 °C. For SHCa-1 hectorite (Fig. 15), the 1.41 μm feature disappears at 400 °C, and the 1.391 μm band is lost at 800 °C. A new band at 1.365 μm is present in the spectrum of hectorite from 700 to 800 °C. Upon heating to 900 °C all features are lost completely. Saponite and hectorite both exhibit a strong absorption band near 1.91 μm, which gradually becomes weaker with heating. Both saponite and hectorite still have extremely weak 1.91 μm bands upon heating to 900 °C. No major spectral changes are observed for the 2.3 and 2.4 μm bands of saponite and hectorite before these two samples lose these features completely at 800 °C (for hectorite) or 900 °C (for saponite).

The sharp 1.41 μm feature of SBCa-1 beidellite disappears at 400 °C while the 1.399 μm band (Fig. 16a) does not show distinct changes from 100 to 700 °C. At 800 °C, the 1.399 μm band becomes extremely weak and disappears at 900 °C. A new weak band at ~1.366 μm begins to develop for beidellite at 600 °C and is lost at 900 °C. For Syn-1 montmorillonite (Fig. 16b), the 1.407 μm band begins to shift gradually to shorter wavelengths (~1.396 μm at 900 °C) at 400 °C and this shifted feature exists in the spectrum until 900 °C. In addition, a new spectral feature at 1.365 μm is observed to be present in the spectrum from 400 to 900 °C. In the 1.9 μm region, a similar trend to saponite and hectorite is observed for beidellite and Syn-1 montmorillonite, although the 1.9 μm feature of Syn-1 montmorillonite remains strong at 900 °C. Beidellite and Syn-1 montmorillonite both have their 2.2 μm features shifted slightly toward shorter wavelengths with heating. Beidellite loses its M–OH combination feature at 900 °C while Syn-1 montmorillonite still displays a strong absorption band at ~2.17 μm at the same temperature.

3.3.3. Sepiolite–palygorskite group

PFl-1 palygorskite's spectral bands (Fig. 17a) occurring at 1.38 and 1.41 μm change significantly at 500 °C; the 1.41 μm feature is lost and two new spectral features appear at 1.366 and 1.370 μm. The 1.366 μm band is still present in the 900 °C spectrum while the 1.370 μm feature disappears upon heating to 700 °C. SepSp-1 sepiolite (Fig. 17b) displays three spectral features at 1.38, 1.39, and 1.42 μm. They show different behaviors upon

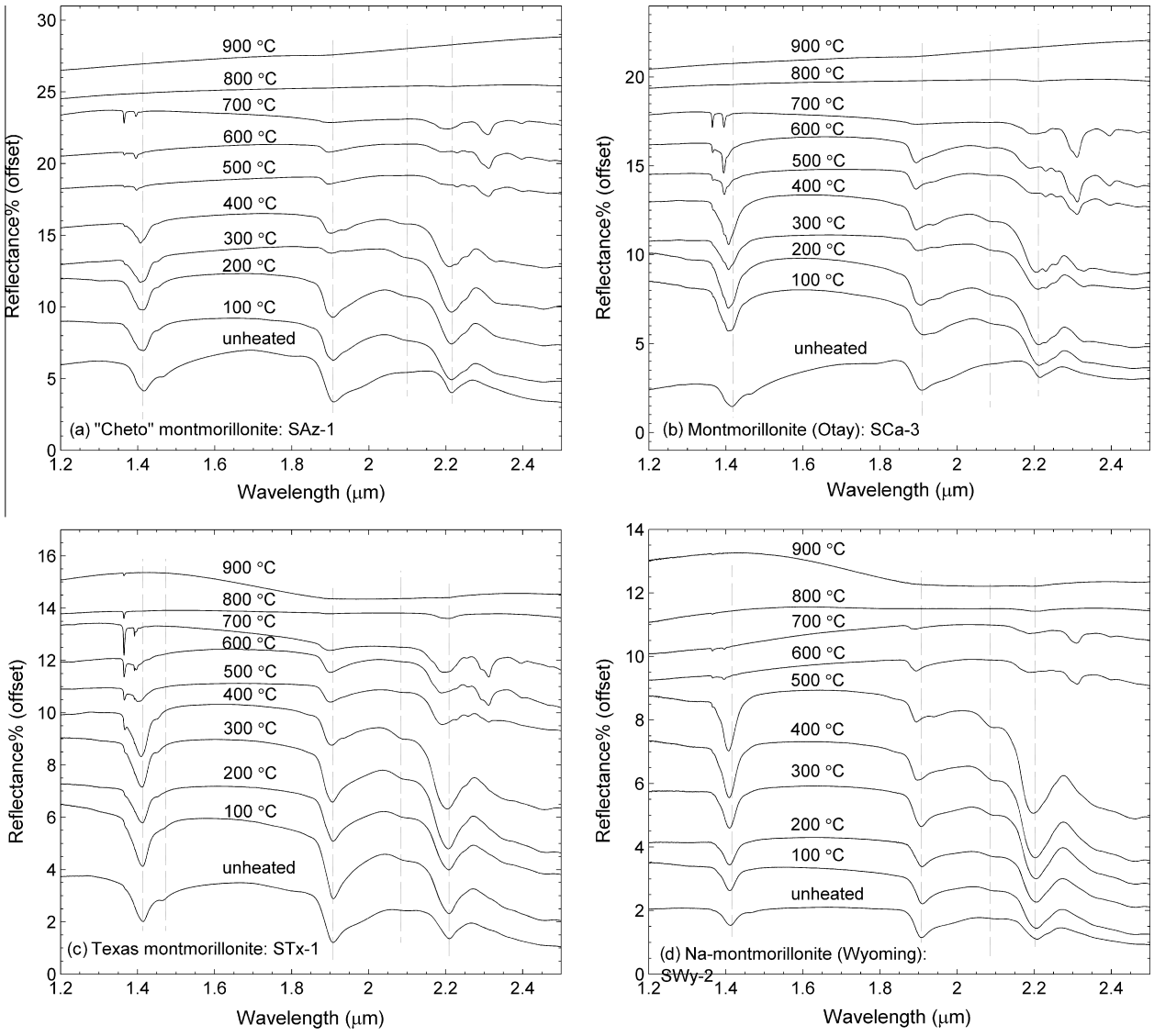

Fig. 12. (a) 1.2–2.5 μm diffuse reflectance spectra of "Cheto" montmorillonite (SAz-1) calcined at various temperatures. (b) 1.2–2.5 μm diffuse reflectance spectra of montmorillonite (Otay) (SCa-3) calcined at various temperatures. (c) 1.2–2.5 μm diffuse reflectance spectra of Texas montmorillonite (STx-1) calcined at various temperatures. (d) 1.2–2.5 μm diffuse reflectance spectra of Na-montmorillonite (Wyoming) (SWy-2) calcined at various temperatures. Linear vertical offset is applied to the spectra for clarity.

heating: the 1.42 μm band becomes broad and weak at 400 °C and disappears at 700 °C; the 1.39 μm feature is present as a strong absorption in the 700 °C spectrum and disappears completely at 800 °C; the 1.38 μm feature disappears at 700 °C. In addition, a new band at 1.364 μm starts to develop at 600 °C and becomes a strong absorption band at 900 °C. The 1.92 μm bands of palygorskite and sepiolite decrease gradually in intensity and shift slightly to shorter wavelengths with heating, but these features are still detectable at 900 °C. Playgorskite's original spectral features near 2.2 μm are replaced by 2.19 and 2.31 μm bands at 400 °C. Upon heating to 800 °C and 900 °C, only a broad spectral absorption centered at ~2.21 μm is observed for playgorskite. In the case of sepiolite, there are multiple spectral features in the range 2.2–2.4 μm. These bands are not strongly affected by temperatures as high as 700 °C. At 800 and 900 °C, only one broad band at 2.21 μm is present in the sepiolite spectrum.

3.3.4. Chlorite group

Clinochlore's 1.39 μm feature is not affected by heating until 800 °C (Fig. 18), at which point this feature disappears completely. The 1.45 μm band, however, is affected significantly by heating, disappearing completely at 500 °C. Two absorption features due to combination modes of H_2O occur in the 1.9–2.0 μm range. These two bands become weak at 500 °C, and then completely disappear at 800 °C. Clinochlore also has multiple features present in the 2.2–2.4 μm range. Although these spectral bands shift slightly away from their original positions with heating, they do not show major changes before their complete disappearance at 800 °C.

3.3.5. Zeolite group

Two natural zeolites in this study exhibit weak absorption bands in the 2.2–2.4 μm region (Fig. 19a and b). Given that zeolites do not have OH in their structures, the spectral features in this region may be due to the occurrence of M-OH combination modes occurring when a small amount of H_2O hydrogen atoms bond to extraframework (K^+, Ca^{2+}, and Na^+) and tetrahedral (Si^{4+}, Al^{3+}) cations (Cloutis et al., 2002). These features are very weak, but they remain in the spectra when heated to 800 °C (clinoptilolite) or 900 °C (mordenite). No distinct changes in the 1.9 region of mordenite and clinoptilolite occur before a significant decrease in

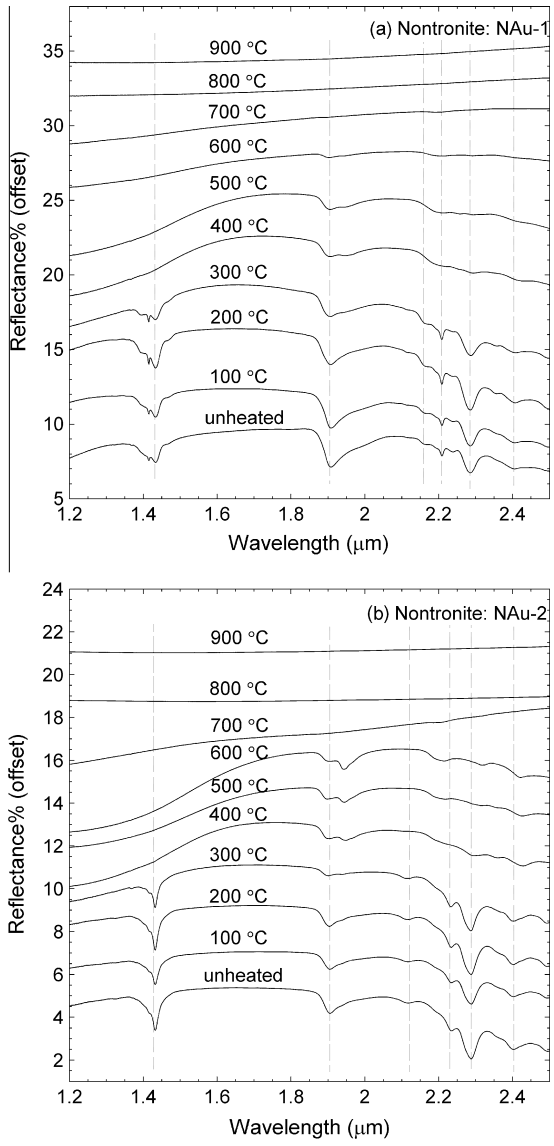

Fig. 13. (a) 1.2–2.5 μm diffuse reflectance spectra of nontronite (NAu-1) calcined at various temperatures. (b) 1.2–2.5 μm diffuse reflectance spectra of nontronite (NAu-2) calcined at various temperatures. Linear vertical offset is applied to the spectra for clarity.

intensity of the 1.91 μm band at 800 °C (for clinoptilolite) or 900 °C (for mordenite). Clinoptilolite and mordenite both exhibit strong absorption bands near 1.42 μm. The shape and position of this feature is not affected by heating before the complete disappearance of this band at 800 °C for clinoptilolite and 900 °C for mordenite. The extremely weak spectral feature near 1.365 μm of both natural zeolites is present in their spectra until 800 °C.

3.3.6. Other observations

Fourteen of the samples studied here exhibit an absorption feature near 1.365 μm when samples are heated to temperatures between 400 and 900 °C. The temperature range over which this non-diagnostic feature occurs as well as its intensity are different for each sample. Kaolinite (Fig. 11) exhibits a very weak 1.367 μm band from 400 °C to 900 °C. Among the montmorillonites, SAz-1 (Fig. 12a) and SCa-3 (Fig. 12b) have new 1.366 μm features with comparable intensities from 500 to 700 °C, and 1.366 μm bands appear from 400 to 800 °C and 600 to 800 °C for

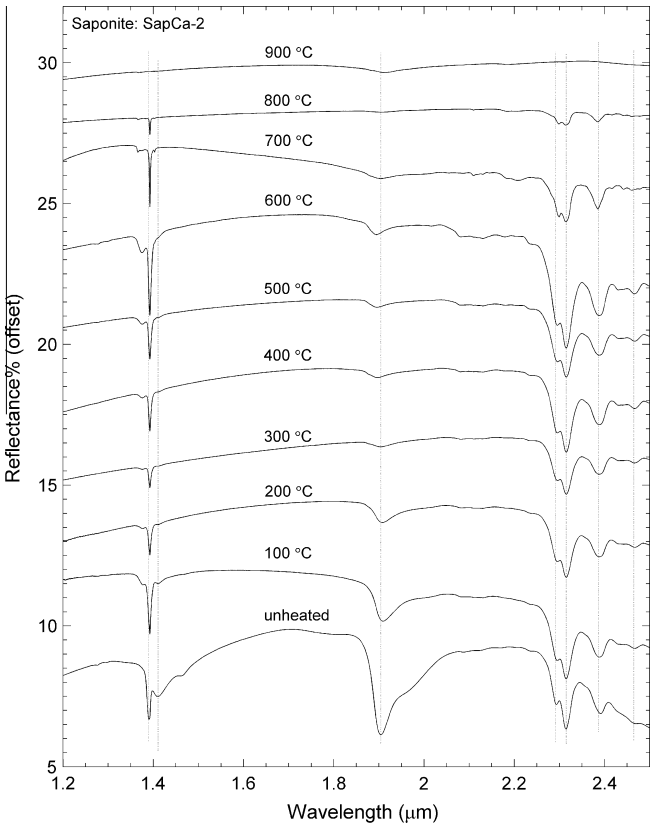

Fig. 14. 1.2–2.5 μm diffuse reflectance spectra of saponite (SapCa-2) calcined at various temperatures. Linear vertical offset is applied to the spectra for clarity.

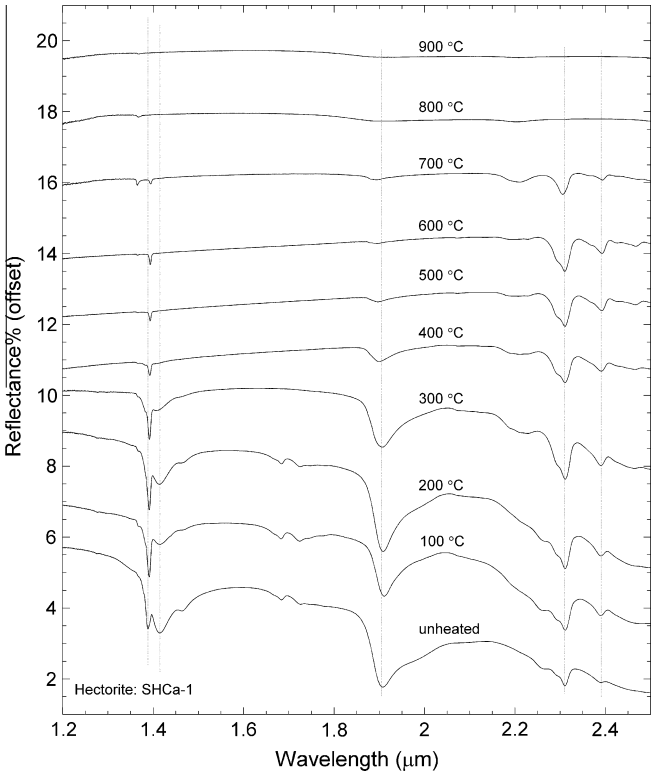

Fig. 15. 1.2–2.5 μm diffuse reflectance spectra of hectorite (SHCa-1) calcined at various temperatures. Linear vertical offset is applied to the spectra for clarity.

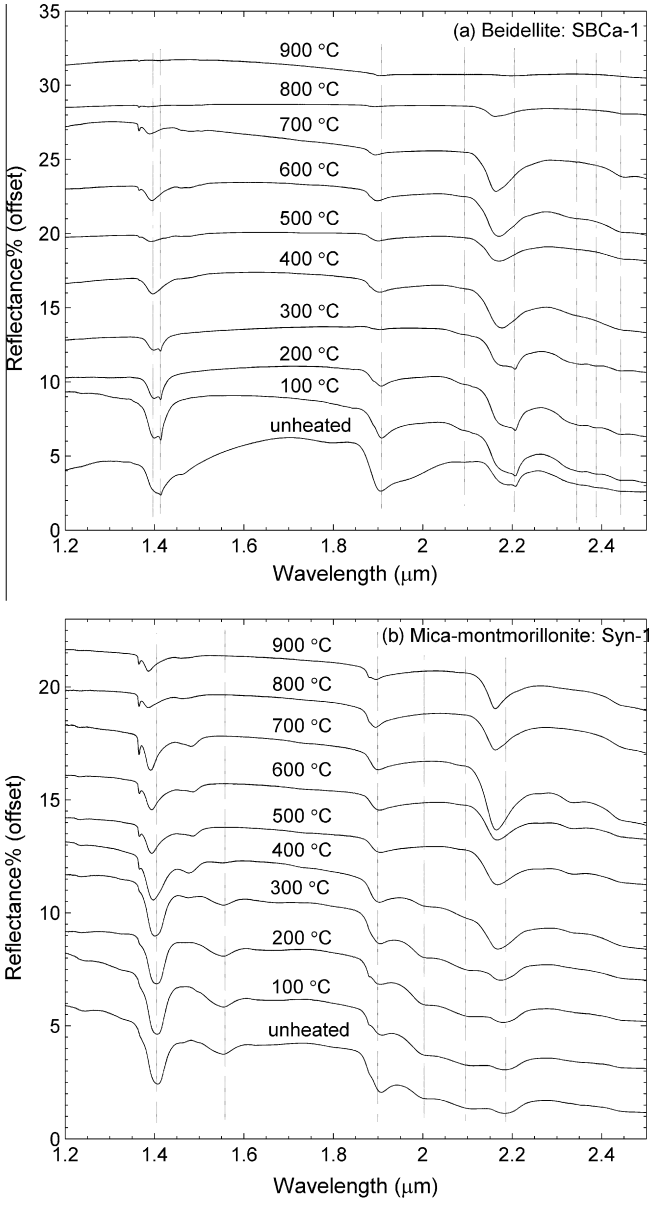

Fig. 16. (a) 1.2–2.5 μm diffuse reflectance spectra of beidellite (SBCa-1) calcined at various temperatures. (b) 1.2–2.5 μm diffuse reflectance spectra of mica-montmorillonite (Syn-1) calcined at various temperatures. Linear vertical offset is applied to the spectra for clarity.

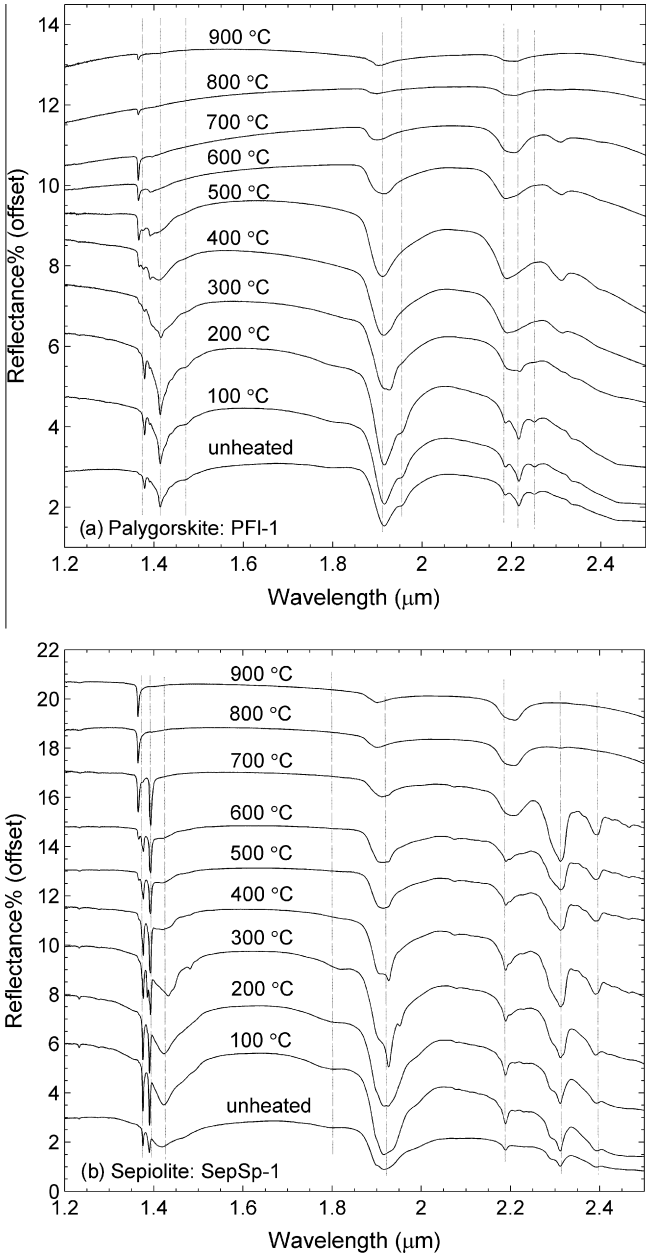

Fig. 17. (a) 1.2–2.5 μm diffuse reflectance spectra of palygorskite (PFl-1) calcined at various temperatures. (b) 1.2–2.5 μm diffuse reflectance spectra of sepiolite (SepSp-1) calcined at various temperatures. Linear vertical offset is applied to the spectra for clarity.

STx-1 (Fig. 12c) and SWy-2 (Fig. 12d), respectively. Saponite (Fig. 14) and hectorite (Fig. 15) exhibit recognizable 1.365 μm bands only at 700 °C. An extremely weak 1.366 μm feature is observed for beidellite (Fig. 16a) from 600 to 800 °C. For Syn-1 montmorillonite (Fig. 16b), a 1.365 μm band appears at 500 °C and develops as an absorption band with detectable intensity at 900 °C. Palygorskite (Fig. 17a) and sepiolite (Fig. 17b) both exhibit this new feature from 500 to 900 °C. The 1.364 μm band of sepiolite develops as a very strong feature at 900 °C. In the case of clinochlore (Fig. 18), an extremely weak 1.364 μm band is present from 600 to 800 °C. In the case of two natural zeolites (Fig. 19a and b), the untreated samples already exhibit weak 1.365 bands and their bands are still present in the spectra upon heating to 900 °C. However, for Fe-rich nontronites (Fig. 13a and b), such spectral features do not appear at all. Nontronites lose their 1.4 μm features completely at 400 °C and no new spectral bands form during following heating treatment.

4. Discussion

4.1. Effects of thermal behaviors of phyllosilicates and natural zeolites

The integration of mid-to-far-IR emissivity and NIR reflectance spectral results along with DSC results of phyllosilicates and natural zeolites allow us to conclude that, in general, the diverse spectral changes observed in this study are significantly affected by samples' thermal behaviors.

4.1.1. Kaolinite group

There is no endothermic peak observed in DSC curve of kaolinite associated with the loss of adsorbed and interlayer H_2O, because kaolinite contains no structural H_2O (e.g., Farmer, 1974; Bailey, 1980). Kaolinite's first endothermic reaction, which is caused by

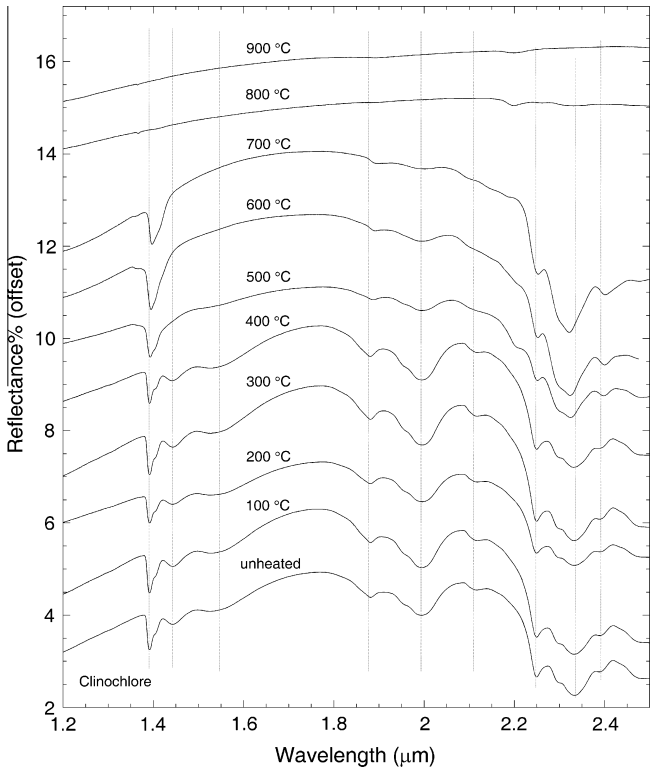

Fig. 18. 1.2–2.5 μm diffuse reflectance spectra of clinochlore calcined at various temperatures. Linear vertical offset is applied to the spectra for clarity.

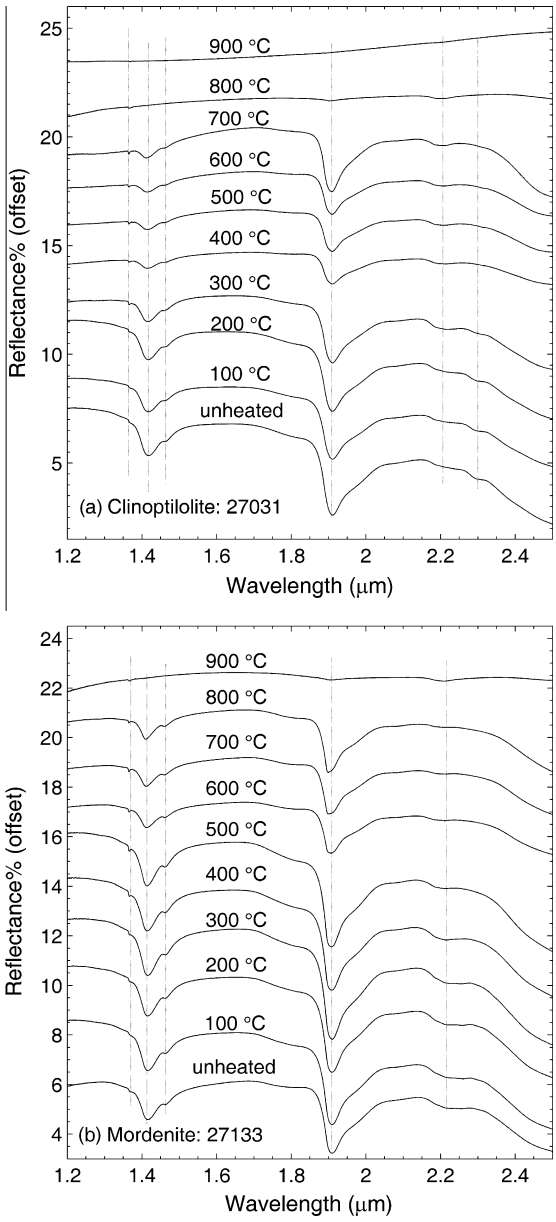

Fig. 19. (a) 1.2–2.5 μm diffuse reflectance spectra of clinoptilolite (27,031) calcined at various temperatures. (b) 1.2–2.5 μm diffuse reflectance spectra of mordenite (27,133) calcined at various temperatures. Linear vertical offset is applied to the spectra for clarity.

removal of structural OH (Holdridge and Vaughan, 1957), occurs in the temperature range 460–600 °C (Fig. 1a). Correspondingly, all spectral features observed for kaolinite change significantly at 400 °C and new bands related to heating products remain up to 900 °C (Figs. 2 and 11). This consistency suggests the dehydroxylation process of kaolinite is the reason leading to its major spectral change. Kaolinite displays a second strong endothermic effect centered at ~830 °C, which has been previously interpreted as being caused by transition from a more-ordered structure to a less-ordered amorphous alumina (Holdridge and Vaughan, 1957). This transition may contribute to the distinct narrowing of kaolinite's major spectral features observed at 800 °C in the mid-to-far-IR region (Fig. 2). This reaction, however, does not affect kaolinite's spectral properties in the NIR region (Fig. 11).

4.1.2. Smectite group

In this study, we analyzed 10 samples from the smectite structural group. Minerals of the smectite group are characterized by 2:1 (one octahedral sheet is linked to a tetrahedral sheet on each side) layers with OH associated with octahedral cations and H_2O molecules in their interlayer region (e.g., Farmer, 1974; Bailey, 1980). Our results exhibit a large variety of spectral changes among the smectite samples.

In general, all montmorillonite samples (SAz-1, SCa-3, STx-1, and SWy-2) display two notable changes in both NIR reflectance and mid-to-far-IR emissivity spectra (Figs. 3 and 12). Based on the investigation of the thermal behaviors by DSC analysis (Fig. 1b–e), the IR properties of montmorillonites are largely affected by their dehydroxylation processes. All montmorillonites show their first endothermic peak in the range 120–140 °C, due to the loss of H_2O (Greene-Kelly, 1957). However, neither their NIR nor the mid-to-far-IR major spectral bands display distinct changes upon heating to this temperature. At ~550 °C a second endothermic reaction commences and ends at ~750 °C, which is followed immediately by a third endothermic effect centered at ~850–900 °C. These two endothermic peaks are interpreted as being due to the loss of structural OH groups and breakdown of the anhydrous montmorillonite to an "amorphous" phase (Greene-Kelly, 1957), respectively. By comparing the IR spectra of montmorillonites upon heating to their DSC results, we account for the two distinct spectral changes occurring at 500–600 °C and 800 °C associated with dehydroxylation of the montmorillonites and collapse of montmorillonites' layer structure, respectively. Upon further heating to ~1000 °C, an exothermic peak is observed for both SAz-1 and SCa-3 montmorillonites (Fig. 1b and c). This reaction was interpreted as formation of new high temperature phases, which may include cristobalite, sillimanite, enstatite, and some amorphous phases (e.g., Greene-Kelly, 1957; Gavin and Chevrier, 2010). Correspondingly, the mid-to-far-IR spectra of SAz-1 and SCa-3 samples show notable changes at 900 °C (Fig. 3a

and b), probably due to the formation of a new crystal structure. The STx-1 and SWy-2 montmorillonites behave differently from the previous two montmorillonites. Neither the DSC (Fig. 1d and e) nor the IR results (Fig. 3c and d) show the formation of new phases at 900 °C. High Mg^{2+} concentration (Table 2) might be the reason leading to the significant spectral change at 900 °C for SAz-1 and SCa-3; previous studies (e.g., Earley et al., 1953; Greene-Kelly, 1957; Gavin and Chevrier, 2010) have concluded that a minor enstatite ($MgSiO_3$) structure begins to form at ~900 °C for Mg^{2+}-rich smectites while other high temperature phases appear upon heating to 1000 °C.

Both nontronite samples (NAu-1 and NAu-2) display a dehydration peak in the 110–135 °C range and a less-pronounced dehydroxylation endothermic peak in the ~500–700 °C region (Fig. 1f and g). Similar to montmorillonite, loss of H_2O does not lead to distinct IR spectral changes. Given the results that all spectral features of nontronites show significant change at 400 °C (Figs. 4 and 13), dehydroxylation may be the major factor affecting nontronite's IR properties.

The first endothermic peak (Fig. 1h and i) of both saponite and hectorite is centered at ~135 °C, due to the removal of H_2O (Greene-Kelly, 1957; Vicente et al., 2001). Similar to all of the smectite samples discussed above, the IR spectral features (Saponite: Figs. 5 and 14; hectorite: Figs. 6 and 15) of both samples are not substantially affected by dehydration reactions. However, the 1.41 μm and 1.9 μm features of saponite and hectorite show a decrease in intensity at 100 °C, and the weak 1.95 μm shoulder band of both samples disappears at 100 °C. At higher temperatures (~800–950 °C for saponite, ~600–850 °C for hectorite), an endothermic–exothermic inversion occurs for these two samples, indicating the removal of structural hydroxyl groups followed by a phase change (Greene-Kelly, 1957; Vicente et al., 2001). This high temperature phase of saponite and hectorite has been determined by previous investigators (e.g., Kulbicki, 1959; Green et al., 1970; Kloprogge et al., 2000; Kloprogge and Frost, 2000) and confirmed in our previous XRD studies (Che et al., 2011) to be enstatite ($MgSiO_3$). The mid-to-far-IR emissivity spectral results of both samples are in good agreement: saponite and hectorite display completely different spectral features from their original bands at temperatures higher than 700 °C. In addition, NIR spectra of both samples reveal more detailed information of their thermal behaviors. Saponite keeps its hydration spectral features at 800 °C while the 800 °C hectorite spectrum has already become featureless. This behavior is in agreement with the fact that saponite shows an endothermic–exothermic inversion at a higher temperature range than hectorite does in their DSC curves. Therefore, the IR properties of these two samples are significantly affected by dehydroxylation and recrystallization reactions.

Similar to the montmorillonites, beidellite and Syn-1 montmorillonite both exhibit three main endothermic peaks (Fig. 1j and k) near 120 °C, 540 °C, and 800–900 °C, which are attributed to the loss of H_2O, loss of structural hydroxyl groups, and collapse of the layer structure, respectively (Greene-Kelly, 1957). Spectral bands of beidellite and Syn-1 montmorillonite do show a slight shift from their original positions with increasingly higher temperature (Figs. 7 and 16). However, these two minerals' major spectral bands are resistant to changes at temperatures as high as 800 °C for beidellite and 900 °C for Syn-1 montmorillonite. The dehydration process occurring in the temperature range 100–200 °C, as observed in the DSC analysis, does not affect the IR spectral properties of these two samples distinctly. The dehydroxylation reaction begins at 400–500 °C, which may be responsible for the minor change of IR spectra of beidellite and Syn-1; a few of their spectral features shift slightly away from the original positions in this temperature range. Neither of these last two effects, however, strongly alters their IR spectra. Finally, the third endothermic reaction near 810 °C is correlated with a major change in beidellite's IR spectrum, as beidellite loses all of its original spectral features at 900 °C. For Syn-1, the third endothermic effect occurs at ~930 °C, therefore, neither the mid-to-far-IR nor NIR spectrum changes distinctly at 900 °C.

Of all the smectites studied here, the major differences among them are compositions of the octahedral cations. Montmorillonite and nontronites are Al^{3+}, and Fe^{3+}-rich dioctahedral smectites; beidellite and Syn-1 montmorillonite are significantly rich in Al^{3+}; hectorite and saponite are Mg^{2+}-rich trioctahedral smectites. These differences may yield the variable spectral behaviors we have observed among the smectite minerals, and further discussion appears in the next section.

4.1.3. Sepiolite–Palygorskite group

The structure represented by palygorsktie and sepiolite is composed of octahedral and tetrahedral sheets that are divided into ribbons by inversion. The tetrahedral sheets are still linked and alternating channels are formed by this ribbon-like morphology, while the alternating channels between ribbon strips are occupied by H_2O molecules and exchangeable cations (e.g., Farmer, 1974; Bailey, 1980). Palygorskite and sepiolite both have several forms of H_2O present inside their structure. For palygorskite, there are H_2O molecules attached to octahedral cations, a small amount of zeolitic H_2O (that is coordinated with a cation on the exchange sites in the interlayers of phyllosilicates and within the cages of zeolites (e.g., Ming et al., 2008)) in channels, and H_2O groups situated laterally along the channels. Sepiolite has a similar structure except most H_2O exists in its channels as zeolitic H_2O (e.g., Bailey, 1980). Consequently, both DSC (Fig. 1l and m) and IR results (Figs. 8 and 17) show that palygorskite and sepiolite have more complicated thermal behaviors compared to the other samples in this study. In the temperature range of 50–550 °C, palygorskite displays several weak endothermic peaks (~100 °C, ~140 °C, ~230 °C, and ~480 °C) reflecting the dehydration and dehydroxylation reactions (Caillere and Henin, 1957a). IR spectra of palygorskite agree well with the DSC curve by showing spectral changes at 300, 400, and 500 °C. Upon heating to ~880 °C, an endothermic–exothermic inversion appears in DSC curve of palygorskite, reflecting a recrystallization into enstatite (e.g., Kulbicki, 1959; Caillere and Henin, 1957a). Correspondingly, IR spectra of palygorskite in both mid-to-far-IR and NIR regions show major changes at 800 °C. However, no characterized enstatite spectral features (compared to the enstatite emissivity spectrum in Hamilton et al., 1997) are observed in palygorskite's 900 °C emissivity spectrum. It is possible that only minor enstatite structure forms at the temperature of 900 °C. Similar to palygorskite, the DSC curve of sepiolite is also composed of several endothermic peaks in the low temperature range (~110 °C, 330 °C, and 590 °C) associated with dehydration and dehydroxylation reactions, and an endothermic–exothermic inversion near 840 °C due to the crystallization of enstatite (e.g., Kulbicki, 1959; Caillere and Henin, 1957a). The exothermic peak of sepiolite, however, is significantly stronger than that of palygorskite. The IR spectra of sepiolite are in good agreement with the sample's thermal behaviors showed by DSC analysis. The spectral features, especially sepiolite's hydration spectral bands, display several distinct changes in the temperature range 25–500 °C. The mid-to-far-IR spectra reveal the formation of enstatite at 800 °C for sepiolite by displaying completely different spectral features from those of unheated sepiolite. The major features of 800 and 900 °C emissivity spectra match well with the spectral bands of enstatite recorded in Arizona State University Spectral Library (spectrum ID: 537).

4.1.4. Chlorite group

Clinochlore only has hydroxyls in its structure. However, there are two types of OH present: one is coordinated to octahedral cations and the other is associated with the $(R^{2+}, R^{3+})_3(OH)_6$ (R is an octahedral cation such as Fe^{2+}, Mg^{2+}, Zn^{2+}, or Al^{3+}) octahedral sheet in the interlayers (e.g., Farmer, 1974; Bailey, 1980). The DSC curve of clinochlore (Fig. 1n) shows corresponding results by giving two strong endothermic peaks. The first endothermic peak in the ~500–650 °C region represents the decomposition of the brucite layer in its interlayer and the second one in the ~800–900 °C range is due to the dehydroxylation of sample's layer structure (Caillere and Henin, 1957b). Previous studies (Villieras et al., 1994) have concluded that clinochlore transforms to "modified chlorite" termed by Villieras et al. (1994) at 500 °C, then at 800 °C new phases olivine and spinel start to form (e.g., Brindley and Ali, 1950). The IR spectra of clinochlore (Figs. 9 and 18) agree well with the thermal behavior determined by DSC measurement: two distinct changes occurring at 500 °C and 800 °C are observed in both the NIR and mid-to-far-IR spectral results. Therefore, as each phase of dehydroxylation is taking place, the IR properties of clinochlore show major changes.

4.1.5. Zeolite group

Phyllosilicates exhibit a wide variety of significant spectral changes as temperature is increased. However, the mid-to-far-IR emissivity spectra of clinoptilolite and mordenite show no obvious change upon heating (Figs. 10 and 19). The shapes and locations of the NIR spectral bands are not affected by thermal treatment before the completion of dehydration. These spectral results are consistent with the fact that zeolites all have three-dimensionally linked and rigid crystal structures (e.g., Breck, 1974b; Barrer, 1978, 1982; Newsam, 1986; Armbruster and Gunter, 2001), that are more stable than the layer structures of phyllosilicates. DSC curves of both zeolites (Fig. 1o and p) reveal more detailed information of their thermal properties. The first endothermic peak of clinoptilolite and mordenite occurred near 110 °C, corresponding to the loss of large amount H_2O from their crystal structures (Földesová et al., 1999; Alver et al., 2010). However, neither the mid-to-far-IR nor the NIR spectral features are affected by this dehydration reaction. The endothermic peaks occurring at higher temperatures (~690 °C for clinoptilolite and ~810 °C for mordenite) may reflect the collapse of the zeolite structure (Földesová et al., 1999; Alver et al., 2010). NIR spectra of the two zeolites are in good agreement with this high temperature reaction: clinoptilolite tends to lose all its hydration features at 800 °C and the spectrum of mordenite becomes featureless at 900 °C. However, corresponding changes are not observed in zeolites' mid-to-far-IR spectra.

4.2. Effects of octahedral cations

The IR spectral features of phyllosilicates are affected by their octahedral cations because different cations need different energies to pull charge away from hydroxyls (e.g., Bishop et al., 2008). Previous investigators also observed that the position of the M–O–Si absorption appears to be linearly related to the average ionic radius of the cations in phyllosilicates' octahedral sites. The wavenumber position decreases in the order $Al^{3+} > Al^{3+}/Fe^{3+} > Fe^{3+} > Mg^{2+}$ (e.g., Michalski et al., 2005). Our results indicate that this order is also suitable to describe the IR spectral stability of phyllosilicates. Spectral bands of Al^{3+}-rich smectites are less affected by high temperatures than those of Fe^{3+}-smectites. The stability of Al^{3+}-rich smectites decreases as their Al^{3+} abundance decreases. Montmorillonites SAz-1 (Al/Si = 0.33), SCa-3 (Al/Si = 0.22), and STx-1 (Al/Si = 0.25) display their first distinct spectral changes in both NIR reflectance and mid-to-far-IR emissivity spectra at 500 °C (Figs. 3a–c and 12a–c). SWy-2 (Al/Si = 0.36), however, shows its first obvious change at 600 °C (Figs. 3d and 12d). In the case of beidellite (Al/Si = 0.6), its original mid-to-far-IR emissivity and NIR reflectance spectra are changed significantly only at 900 °C (Figs. 7a and 16a). Before 900 °C, the major spectral change in beidellite is related to a slight shifting of original spectral bands (to both longer and shorter wavelengths). Syn-1 montmorillonite (Al/Si = 0.77) exhibits the strongest resistance to high temperature by maintaining the OH/H_2O overtone and combination bands at temperature as high as 900 °C (Figs. 7b and 16b). In addition, Syn-1's emissivity spectra do not show a conspicuous change upon heating to 900 °C. Nontronites with a high Fe^{3+} abundance, however, lose all original spectral features in the mid-to-far-IR and NIR regions at 400 °C (Figs. 4 and 13). In addition, no NIR spectral band is observed for nontronite at 700 °C while the other smectite minerals all retain distinct spectral bands upon heating to 700 °C.

The spectral features of phyllosilicates with a certain amount (Mg/Si = ~0.11–0.96) of Mg^{2+} show unique behavior during thermal treatments. For the trioctahedral phyllosilicates hectorite (Mg/Si = 0.43), saponite (Mg/Si = 0.46), clinochlore (Mg/Si = 0.96), and sepiolite (Mg/Si = 0.41), mid-to-far-IR emissivity spectra at 700 °C display evidence for the formation of new phases (Figs. 5, 6, 8b and 9), which were determined to be enstatite (olivine + spinel for clinochlore) by previous studies (e.g., Brindley and Ali, 1950; Kulbicki, 1959). The same transformation occurred for clinochlore and sepiolite at 800 °C. These new spectral features are completely different from the familiar phyllosilicate features that dominate Si–O stretching and bending bands. For montmorillonites SAz-1 (Mg/Si = 0.11), SCa-3 (Mg/Si = 0.15), and palygorskite (Mg/Si = 0.18), the presence of a small amount of Mg^{2+} in their octahedral sites also affect the high temperature spectral behaviors. At 800 °C, a unique spectral band at ~920 cm^{-1} appears and becomes strong and dominant at 900 °C (Figs. 3a, b, and 8a). Given the fact that Mg^{2+}-rich phyllosilicates tend to form new crystal structures at high temperatures, this new band could be due to newly-formed bonds associated with Mg^{2+} and could be a diagnostic spectral feature of high temperature Mg^{2+}-rich dioctahedral phyllosilicates.

4.3. Inconsistency between spectral behaviors in the mid-to-far-IR and NIR regions and geologic implications

One of the important objectives of this study is to determine if thermal treatment could affect the TIR (400–1400 cm^{-1}) and NIR regions in different ways, which could partially be responsible for the difficulty in detecting phyllosilicates on Mars using TIR emission spectroscopy. Results from this study have shown that phyllosilicates can lose all original spectral features in the TIR region while maintaining their characteristic hydration bands in NIR region in the same temperature range.

4.3.1. Nontronite

Michalski et al. (2010) analyzed the nontronite deposits in the Nili Fossae region using TES data. They did not detect the spectral features showing the occurrences of nontronite in long-wavelength region. Instead, TES data consistently exhibit a spectral absorption located near ~450 cm^{-1} on the same surfaces where OMEGA and CRISM data display the diagnostic NIR spectral bands (1.4, 1.9, 2.3, and 2.4 μm) for nontronite. Our laboratory results (Figs. 4 and 13) show that the doublet or triplet spectral feature in the Si–O bending region of nontronites disappear at 400 °C and is replaced by one single absorption centered at ~450 cm^{-1}. In the NIR region, both nontronite samples display the 1.9 μm band and extremely weak 2.3 and 2.42 μm features when heated to 400 °C. We also observe that both nontronites lose the 1.4 μm

feature completely at the 400 °C. Based on the observation from Nili Fossae and spectral results from this study, we suggest that the nontronite deposits in Nili Fossae have been partially altered at temperatures up to 400 °C. This thermally altered nontronite may occur within an assemblage that is composed of both unaltered and thermally altered nontronite along with a variety of other silicate minerals. The NIR spectrum of this assemblage could have a weak 1.4 μm feature, a strong 1.9 μm feature, and the diagnostic 2.3 μm band, while the far-IR region is dominated by a strong 450 cm^{-1} absorption band. This hypothesis will be investigated by detailed future remote sensing study.

4.3.2. Trioctahedral phyllosilicates

As discussed in previous sections, the octahedral sites of trioctahedral phyllosilicates are occupied with Mg^{2+}, and they tend to form the enstatite structure upon heating to 700 °C. In this study, hectorite (Figs. 6 and 15), saponite (Figs. 5 and 14), and sepiolite (Figs. 8b and 17b) all still maintained diagnostic NIR spectral bands of phyllosilicates at high temperatures (e.g. 1.9, 2.3 and 2.4 μm features at 700 °C for hectorite and saponite; 1.9, 2.2 μm bands at 900 °C for sepiolite), while their mid-to-far-IR spectra at temperatures of 700 °C or higher were already dominated by spectral bands of enstatite, which are completely different from those of phyllosilicates.

5. Summary and conclusions

In order to complement mid-to-far-IR studies of dehydrated and/or dehydroxylated phyllosilicates and zeolites (Che et al., 2011) and supplement the spectral library (available at http://aram.ess.sunysb.edu/tglotch/spectra.html) at the Stony Brook University Vibrational Spectroscopy Laboratory, we reported NIR diffuse reflectance and mid-to-far-IR emissivity spectra of 14 phyllosilicates and 2 natural zeolites at various temperatures. DSC measurements were also performed on each sample in order to clarify their thermal activities. We conclude that:

(1) Spectral features in both the NIR and mid-to-far-IR regions of phyllosilicates and natural zeolites are significantly affected by heating. The spectral behavior of each sample is unique and thermal behaviors of phyllosilicates and zeolites showed a great influence on the IR spectra upon heating. In general, the effect of dehydration on the IR properties of all phyllosilicates and zeolites in this study is very small. The major spectral changes to phyllosilicate spectra are associated with dehydroxylation reactions, collapse of layer structures, and/or recrystallization to new phases. The two natural zeolites studied here showed minor spectral changes, corresponding to deformation of the zeolite structure at ~700–900 °C.
(2) The composition of octahedral sites strongly influences the spectral behaviors of phyllosilicates: IR spectra of Al^{3+}-rich smectites are more stable than those of Fe^{3+}-rich smectites; stability of Al^{3+}-rich smectites decreases as the Al^{3+} abundance decreases; spectral behaviors of Mg^{2+}-rich phyllosilicates are distinctly affected by the formation of new crystalline phases near 700 °C; phyllosilicates with a small amount of Mg^{2+} in their octahedral sites all displayed a new spectral band at ~920 cm^{-1} upon heating to 700 °C or higher temperatures.
(3) For future remote sensing of phyllosilicate bearing regions on Mars, both NIR reflectance and mid-to-far-IR emissivity spectral results from this study may contribute towards detecting possible dehydrated and/or dehydroxylated phyllosilicates present on the martian surface.

Acknowledgments

This work was supported by the Mars Fundamental Research Program award #NNX08AN62G made to TDG. Detailed reviews by Dr. Steve Ruff and an anonymous reviewer are greatly appreciated and improved the manuscript.

References

Abramov, O., Kring, D.A., 2005. Impact-induced hydrothermal activity on early Mars. J. Geophys. Res. 110, E12S09. doi:10.1029/2005JE002453.
Alver, B.E., Sakizci, M., Yorukogullari, E., 2010. Investigation of clinoptilolite rich natural zeolites from Turkey: A combined XRF, TG/DTG, DTA and DSC study. J. Therm. Anal. Calorim. 100, 19–26.
Armbruster, T., Gunter, M.E., 2001. Crystal structure of natural zeolites. In: Bish, D.L., Ming, D.W. (Eds.), Natural zeolites: Occurrence, Properties, Application, Reviews in Mineralogy and Geochemistry, vol. 45. Mineralogical Society of America and Geochemical Society, Washington, DC, pp. 1–57.
Bailey, S.W., 1980. Structures of layer silicates. In: Brindley, G.W., Brown, G. (Eds.), Crystal Structures of Clay Minerals and their X-ray Identification. Mineralogical Society, London, pp. 1–124.
Ballet, O., Coey, J.M.D., Burke, K.J., 1985. Magnetic properties of sheet silicates: 2:1:1 layer minerals. Phys. Chem. Miner. 12, 370–378.
Bandfield, J.L., 2002. Global minerals distributions on Mars. J. Geophys. Res. 107 (E6), 5042. doi:10.1029/2001JE001510.
Bandfield, J.L., Hamilton, V.E., Christensen, P.R., 2000. A global view of martian surface compositions from MGS-TES. Science 287, 1626–1630.
Barrer, R.M., 1978. Zeolite frameworks, cations and water molecules. In: Barrer, R.M. (Ed.), Zeolites and Clay Minerals as Sorbents and Molecular Sieves. Academic Press, London, pp. 32–102.
Barrer, R.M., 1982. Occurrence, classification and some properties of zeolites. In: Barrer, R.M. (Ed.), Hydrothermal Chemistry of Zeolites. Academic Press, London, pp. 1–42.
Bibring, J.-P. et al., 2006. Global mineralogical and aqueous Mars history derived from OMEGA/Mars Express data. Science 312, 400–404.
Bish, D.L., 1984. Effects of exchangeable cation composition on the thermal expansion/contraction of clinoptilolite. Clays Clay Miner. 32, 444–452.
Bishop, J.L., Pieters, C.M., Edwards, J.O., 1994. Infrared spectroscopic analyses on the nature of water in montmorillonite. Clays Clay Miner. 42, 701–715.
Bishop, J.L., Lane, M.D., Dyar, M.D., Brown, A.J., 2008. Reflectance and emission spectroscopy study of four groups of phyllosilicates: Smectites, kaolinite–serpentines, chlorites and micas. Clay Miner. 43, 35–54.
Breck, D.W., 1974a. Chemical properties and reactions of zeolites. In: Breck, D.W. (Ed.), Zeolite Molecular Sieves: Structure, Chemistry, and Use. John Wiley and Sons, London, pp. 441–528.
Breck, D.W., 1974b. Structure of zeolites. In: Breck, D.W. (Ed.), Zeolite Molecular Sieves: Structure, Chemistry, and Use. John Wiley and Sons, London, pp. 29–185.
Brindley, G.W., Ali, S.Z., 1950. X-ray study of thermal transformations in some magnesian chlorite minerals. Acta Cryst. 3, 25–30.
Caillere, S., Henin, S., 1957a. The sepiolite and palygorskite minerals. In: Mackenzie, R.C. (Ed.), The Differential Thermal Investigations of Clays. Mineralogical Society, London, pp. 231–247.
Caillere, S., Henin, S., 1957b. The chlorite and serpentine minerals. In: Mackenzie, R.C. (Ed.), The Differential Thermal Investigations of Clays. Mineralogical Society, London, pp. 207–230.
Che, C., Glotch, T.D., Bish, D.L., Michalski, J.R., Xu, W., 2011. Spectroscopic study of the dehydration and/or dehydroxylation of phyllosilicate and zeolite minerals. J. Geophys. Res. 116, E05007. doi:10.1029/2010JE003740.
Cloutis, E.A., Asher, P.M., Mertzman, S.A., 2002. Spectral reflectance properties of zeolites and remote sensing implications. J. Geophys. Res. 107 (E9), 5067. doi:10.1029/2000JE001467.
Earley, J.W., Milne, I.H., McVeagh, W.J., 1953. Dehydration of montmorillonite. Am. Mineral. 38, 770–783.
Ehlmann, B.L. et al., 2009. Identification of hydrated silicate minerals on Mars using MRO-CRISM: Geologic context near Nili Fossae and implications for aqueous alteration. J. Geophys. Res. 114, E00D08. doi:10.1029/2009JE003339.
Fairén, A.G. et al., 2010. Noachian and more recent phyllosilicates in impact craters on Mars. Proc. Natl. Acad. Sci. 107, 12095–12100. doi:10.1073/pnas.1002889107.
Farmer, V.C., 1974. The layer silicates. In: Farmer, V.C. (Ed.), The Infrared Spectra of Minerals. Mineralogical Society, London, pp. 331–363.
Földesová, M., Lukáč, P., Dillinger, P., Balek, V., Svetík, S., 1999. Thermochemical properties of chemically modified zeolite. J. Therm. Anal. Calorim. 58, 671–675.
Frost, R.L., Kloprogge, J.T., 2000. Vibrational spectroscopy of ferruginous smectite and nontronite. Spectrochim. Acta Part A 56, 2177–2189.
Frost, R.L., Kloprogge, J.T., Zhe, D., 2002. The Garfield and Uley nontronites – An infrared spectroscopic comparison. Spectrochim. Acta Part A 58, 1881–1894.
Gaffey, S.J., McFadden, L.A., Nash, D., Pieters, C.M., 1993. Ultraviolet, visible, and near-infrared reflectance spectroscopy: Laboratory spectra of geologic materials. In: Pieters, C.M., Englert, P.A.J. (Eds.), Remote Geochemical Analysis: Elemental and Mineralogical Composition. Cambridge University Press, Cambridge, pp. 43–78.

Gavin, P., Chevrier, V., 2010. Thermal alteration of nontronite and montmorillonite: Implications for the martian surface. Icarus 208, 721–734. doi:10.1016/j.icarus.2010.02.027.

Glotch, T.D., Rossman, G.R., Aharonson, O., 2007. Mid-infrared (5–100 μm) reflectance spectra and optical constants of ten phyllosilicate minerals. Icarus 192, 604–622. doi:10.1016/j.icarus.2007.07.002.

Green, J.M., Mackenzie, K.J.D., Sharp, J.H., 1970. Thermal reactions of synthetic hectorite. Clays Clay Miner. 18, 339–346. doi:10.1346/CCMN.1970.0180606.

Greene-Kelly, R., 1957. The montmorillonite minerals (smectites). In: Mackenzie, R.C. (Ed.), The Differential Thermal Investigations of Clays. Mineralogical Society, London, pp. 140–164.

Hamilton, V.E., Christensen, P.R., McSween Jr., H.Y., 1997. Determination of martian meteorite lithologies and mineralogies using vibrational spectroscopy. J. Geophys. Res. 102, 25593–26603.

Hedley, C.B., Yuan, G., Theng, B.K.G., 2007. Thermal analysis of montmorillonites modified with quaternary phosphonium and ammonium surfactants. Appl. Clay Sci. 35, 180–188.

Holdridge, D.A., Vaughan, F., 1957. The kaolin minerals (kandites). In: Mackenzie, R.C. (Ed.), The Differential Thermal Investigations of Clays. Mineralogical Society, London, pp. 98–139.

Keeling, J.L., Raven, M.D., Gates, W.P., 2000. Geology and characterization of two hydrothermal nontronites from weathered metamorphic rock at the Uley graphite mine, South Australia. Clays Clay Miner. 48, 537–548.

Kloprogge, J.T., Frost, R.L., 2000. The effect of synthesis temperature on the FT-Raman and FT-IR spectra of saponites. Vib. Spectrosc. 23, 119–127.

Kloprogge, J.T., Komarneni, S., Yanagisawa, K., Frost, R.L., Fry, R., 1998. Infrared study of some synthetic and natural beidellites. J. Mater. Sci. Lett. 17, 1853–1855.

Kloprogge, J.T., Frost, R.L., Hickey, L., 1999a. Infrared absorption and emission study of synthetic mica–montmorillonite in comparison to rectorite, beidellite and paragonite. J. Mater. Sci. Lett. 18, 1921–1923.

Kloprogge, J.T., Fry, R., Frost, R.L., 1999b. An infrared emission spectroscopic study of the thermal transformation mechanisms in Al_{13}-pillared clay catalysts with and without tetrahedral substitutions. J. Catal. 184, 157–171.

Kloprogge, J.T., Frost, R.L., Hickey, L., 2000. Infrared emission spectroscopic study of the dehydroxylation of some hectorites. Thermochim. Acta 345, 145–156.

Kulbicki, G., 1959. High temperature phases in sepiolite, attapulgite and saponite. Am. Mineral. 44, 752–764.

Loizeau, D. et al., 2007. Phyllosilicates in the Mawrth Vallis region of Mars. J. Geophys. Res. 112, E08S08. doi:10.1029/2006JE002877.

Madajová, J., Komadel, P., 2001. Baseline studies of the clay minerals society source clays: Infrared methods. Clays Clay Miner. 49, 410–432.

Mangold, N. et al., 2007. Mineralogy of the Nili Fossae region with OMEGA/Mars Express data; 2. Aqueous alteration of the crust. J. Geophys. Res. 112, E08S04. doi:10.1029/2006JE002835.

McDowell, M.L., Hamilton, V.E., 2007a. Phyllosilicate detection and uncertainty from thermal infrared data in the vicinity of the Nili Fossae. Lunar Planet. Sci. 22, 1872 (abstract).

McDowell, M.L., Hamilton, V.E., 2007b. Examination of phyllosilicate-bearing materials in the vicinity of the Nili Fossae using thermal infrared data. Int. Conf. Mars 7, 3095 (abstract).

Mermut, A.R., Faz Cano, A., 2001. Baseline studies of the clay minerals society source clays: Chemical analyses of major elements. Clays Clay Miner. 49, 381–386.

Michalski, J.R., Fergason, R.L., 2009. Composition and thermal inertia of the Mawrth Vallis region of Mars and THEMIS data. Icarus 199, 25–48. doi:10.1016/j.icarus.2008.08.016.

Michalski, J.R., Noe Dobrea, E.Z., 2007. Evidence for a sedimentary origin of clay minerals in the Mawrth Vallis region, Mars. Geology 35, 951–954.

Michalski, J.R., Kraft, M.D., Sharp, T.G., Williams, L.B., Christensen, P.R., 2005. Mineralogical constraints on the high-silica martian surface component observed by TES. Icarus 174, 161–177.

Michalski, J.R., Kraft, M.D., Sharp, T.G., Williams, L.B., Christensen, P.R., 2006. Emission spectroscopy of clay minerals and evidence for poorly crystalline aluminosilicates on Mars from Thermal Emission Spectrometer data. J. Geophys. Res. 111, E03004. doi:10.1029/2005JE002438.

Michalski, J.R., Poulet, F., Bibring, J.-P., Mangold, N., 2010. Analysis of phyllosilicate deposits in Nili Fossae region of Mars: Comparison of TES and OMEGA data. Icarus 206 (1), 269–289. doi:10.1016/j.icarus.2009.09.006.

Milliken, R.E., Mustard, J.F., 2005. Quantifying absolute water content of minerals using near-infrared reflectance spectroscopy. J. Geophys. Res. 110, E12001. doi:10.1029/2005JE002534.

Ming, D.W., Morris, R.V., Clark, B.C., 2008. Aqueous alteration on Mars. In: Bell, J. (Ed.), The Martian Surface – Composition, Mineralogy, and Physical Properties. Cambridge University Press, Cambridge, pp. 519–540.

Newsam, J.M., 1986. The zeolite cage structure. Science 231, 1093–1099.

Post, J.L., 1984. Saponite from near Ballarat, California. Clays Clay Miner. 32, 147–153.

Poulet, F. et al., 2005. Phyllosilicates on Mars and implications for early martian climate. Nature 438, 623–627.

Pruett, R.J., Webb, H.L., 1993. Sampling and analysis of KGa-1b well-crystallized kaolin source clay. Clays Clay Miner. 41, 514–519.

Ruff, S.W., 2003. Basaltic andesite or weathered basalt: A new assessment. Int. Conf. Mars 6, 3258 (abstract).

Ruff, S.W., 2004. Spectral evidence for zeolite in the dust on Mars. Icarus 168, 131–143. doi:10.1016/j.icarus.2003.11.003.

Ruff, S.W., Christensen, P.R., 2007. Basaltic andesite, altered basalt, and a TES-based search for smectite clay minerals on Mars. Geophys. Res. Lett. 34, L10204. doi:10.1029/2007GL029602.

Ruff, S.W., Christensen, P.R., Barbera, P.W., Anderson, D.L., 1997. Quantitative thermal emission spectroscopy of minerals: A technique for measurement and calibration. J. Geophys. Res. 102, 14899–14913.

Salisbury, J.W., 1993. Mid-infrared spectroscopy: Laboratory data. In: Pieters, C.M., Englert, P.A.J. (Eds.), Remote Geochemical Analysis: Elemental and Mineralogical Composition. Cambridge University Press, Cambridge, pp. 79–98.

Salisbury, F.B., Wald, A., D'Aria, D.M., 1994. Thermal-infrared remote sensing and Kirchhoff's law 1. Laboratory measurements. J. Geophys. Res. 99 (B6), 11897–11911.

Schwenzer, S.P., Kring, D.A., 2009. Impact-generated hydrothermal systems capable of forming phyllosilicates on Noachian Mars. Geology 37, 1091–1094.

Van der Marel, H.W., Beutelspacher, H., 1976. Atlas of Infrared Spectroscopy of Clay Minerals and their Admixtures. Elsevier Scientific Pub. Co., Amsterdam, New York.

Van Olphen, H., Fripiat, J.J., 1979. Data Handbook for Clay Materials and other Non-Metalic Minerals. Pergamon, Oxford.

Vicente, M.A., Bañares-Muñoz, M.A., Gandía, L.M., Gil, A., 2001. On the structural changes of a saponite intercalated with various polycations upon thermal treatments. Appl. Catal., A 217, 191–204.

Villieras, F., Yvon, J., Cases, J.M., De Donato, P., Lhote, F., Baeza, R., 1994. Development of microporosity in clinochlore upon heating. Clays Clay Miner. 42 (6), 679–688. doi:10.1346/CCMN.1994.0420604.

Viviano, C.E., Moersch, J.E., 2011. Using THEMIS to address discrepancies between OMEGA/CRISM and TES detections of phyllosilicates. Lunar Planet. Sci. XLII, 2251 (abstract).